

1 Picturing and modeling catchments by representative 2 hillslopes

3 Ralf Loritz¹, Sibylle K. Hassler¹, Conrad Jackisch¹, Niklas Allroggen², Loes van Schaik³,
4 Jan Wienhöfer¹, and Erwin Zehe¹

5 ¹ Karlsruhe Institute of Technology (KIT), Institute of Water and River Basin
6 Management, Karlsruhe, Germany

7 ² University of Potsdam, Institute of Earth and Environmental Science, Potsdam,
8 Germany

9 ³ Technical University Berlin, Institute of Ecology, Berlin, Germany

10

11 *Correspondence to:* Ralf Loritz (Ralf.Loritz@kit.edu)

12 **Abstract:** This study explores the suitability of a single hillslope as most parsimonious
13 representation of a catchment in a physically-based model. We test this hypothesis by
14 picturing two distinctly different catchments in perceptual models and translating these
15 pictures into parametric setups of 2-D physically-based hillslope models. The model
16 parametrizations are based on a comprehensive field data set, expert knowledge and
17 process-based reasoning. Evaluation against stream flow data highlights that both models
18 predicted the annual pattern of stream flow generation as well as the hydrographs
19 acceptably. However, a look beyond performance measures revealed deficiencies in
20 streamflow simulations during the summer season and during individual rainfall-runoff
21 events as well as a mismatch between observed and simulated soil water dynamics. Some
22 of these shortcomings can be related to our perception of the systems and to the chosen
23 hydrological model, while others point to limitations of the representative hillslope
24 concept itself. Nevertheless, our results corroborate that representative hillslope models
25 are a suitable tool to assess the importance of different data sources as well as to
26 challenge our perception of the dominant hydrological processes we want to represent
27 therein. Consequently, these models are a promising step forward in the search of the
28 optimal representation of catchments in physically-based models.

29

30

31 **1 Introduction**

32 The value of physically-based hydrological models has been doubted (e.g. Beven, 1989,
33 Savenije and Hrachowitz, 2016) since their idea was introduced by Freeze and Harlan
34 (1969). Physically-based models like MikeShe (Refsgaard and Storm, 1995) or CATHY
35 (Camporese et al., 2010) typically rely on the Darcy-Richards concept for soil water
36 dynamics, the Penman–Monteith equation for soil-vegetation-atmosphere exchange
37 processes and hydraulic approaches for overland and stream flow. Each of these concepts
38 is subject to limitations arising from our imperfect understanding of the related processes
39 and is afflicted by the restricted transferability of process descriptions from idealized
40 laboratory conditions to heterogeneous natural systems (Grayson et al., 1992; Gupta et
41 al., 2012).

42 Nevertheless the usefulness of physically-based models as learning tool to explore how
43 internal patterns and processes control the integral behavior of hydrological systems, has
44 been corroborated in several studies. For example Pérez et al. (2011) used
45 Hydrogeosphere (Brunner and Simmons, 2012) together with a regularization scheme for
46 its calibration, to infer how changes in agricultural practices affect the stream flow
47 generation in a catchment. Hopp and McDonnell (2009) explored the role of bedrock
48 topography on the runoff generation using HYDRUS 3D (Simunek et al., 2006) at the
49 Panola hillslope. Coenders-Gerrits et al. (2013) used the same model structure to examine
50 the role of interception and slope on the subsurface runoff generation. Bishop et al.
51 (2015), Wienhöfer and Zehe (2014) and Klaus and Zehe (2011) used physically-based
52 models to investigate the influence of vertical and lateral preferential flow networks on
53 subsurface water flow and solute transport, including the issue of equifinality and its
54 reduction. These and other studies (e.g. Ebel et al., 2008, Scudeler et al., 2016) show that
55 physically-based models can be set up using a mix of expert knowledge and observed
56 parameters and may be tested against a variety of observations beyond stream flow – such
57 as soil moisture observations, groundwater tables or tracer break-through curves. Such
58 studies are, on the one hand an option to increase our limited understanding of the
59 processes underlying physically-based models (Loague and VanderKwaak, 2004), and on
60 the other hand reveal if a model allows consistent predictions of dynamics within the
61 catchment and of its integral response behavior (Ebel and Loague, 2006).

62 Setting up a classical physically-based model in a heterogeneous environmental system is,
63 however, a challenge as it requires an enormous amount of highly resolved spatial data,

64 particularly on subsurface characteristics. Such data sets are rare and only available in
65 rather homogeneous systems or in environmental system simulators as Biosphere 2 LEO
66 (Hopp et al., 2009). Therefore, it has been a long standing vision to replace fully
67 distributed physically-based models by aggregated but yet physically-based model
68 concepts for instance the Hillslope Storage Boussinesq approach (HSB, Troch et al.,
69 2003; Berne et al., 2005) or the REW approach (Representative Elementary Watershed
70 e.g. Reggiani and Rientjes, 2005; Zhang and Savenije, 2005). The key challenge in
71 applying these concepts to real catchments is the assessment of a closure relationship,
72 which parameterizes a) hydrological fluxes (Beven, 2006a) and b) soil water
73 characteristics in an aggregated effective manner (Lee et al., 2006; Zehe et al., 2006).
74 Furthermore, is it not completely clear whether the entire range of variability in
75 subsurface characteristics is relevant for hydrological simulations (Dooge, 1986; Zehe et
76 al., 2014). There are, however, promising concepts emerging, for example the work of
77 Hazenberg et al. (2016) who recently developed a hybrid model consisting of the HSB
78 model in combination with a 1-D representation of the Richards equation for the
79 unsaturated zone.

80 Regardless of whether one favors physically-based, hybrid or more statistical model
81 approaches, a perfect representation of a hydrological system should balance the
82 necessary complexity with greatest possible simplicity (Zehe et al., 2014). The former is
83 necessary to avoid oversimplification. The latter attempts to avoid the drawbacks of over-
84 parametrization (Schoups et al., 2008). In principle there are two ways how one can try to
85 reach this optimum model structure. Either by starting with a complex system
86 representation, for instance a full 3-D catchment model and simplify the model structure
87 as much as possible or by starting at the other end of the spectrum, with the most
88 parsimonious model structure and proceed towards higher complexity. In conceptual
89 rainfall-runoff models which follow the HBV concept (Bergström and Forsman, 1973)
90 the most parsimonious model structure for simulating the behavior of a catchment is a
91 single reservoir. In the case of physically-based models there is more than one starting
92 point. In flatland catchments without dominant lateral flow processes in the soil one
93 might choose a single soil column. This “null model” could be refined into multiple
94 parallel acting columns, to capture variability in vegetation and soil properties. This
95 represents the first generation of land surface components in meteorological models (e.g.
96 Niu et al., 2011) and the first generation of models for the catchment scale dynamics of
97 nitrate (Refsgaard et al., 1999).

98 However, in hilly or mountainous terrain the smallest meaningful unit is a hillslope
99 including the riparian zone, because rainfall and radiation input depend on slope and
100 aspect, as well as on downslope gradients which cause lateral fluxes in the unsaturated
101 zone (e.g. Bachmair and Weiler, 2011; Zehe and Sivapalan, 2007). This is the reason why
102 hillslopes are often regarded as the key landscape elements controlling transformation of
103 precipitation and radiation inputs into fluxes and stocks of water (e.g. Bronstert and Plate,
104 1997), energy (Zehe et al., 2010, 2013) and sediments (Mueller et al., 2010).

105 The most parsimonious representation of a small catchment in a physically-based model
106 could thus be a single representative hillslope. However, the challenge of how to identify
107 such a hillslope has rarely been addressed. This reflects the fact that the identifiability of a
108 representative hillslope has been strongly questioned since the idea was born. For
109 example, Beven (2006) argues that neither is the hillslope form uniquely defined nor is it
110 clear whether it is the form that matters, the pattern of saturated areas (Dunne and Black,
111 1970) or the subsurface architecture. The enormous spatial variability of soil hydraulic
112 properties and preferential flow paths in conjunction with process non-linearity are
113 additional arguments against the identifiability of representative hillslope models (Beven
114 and Germann, 2013). Nevertheless, hillslopes act as miniature catchments (Bachmair and
115 Weiler, 2011), which made Zehe et al. (2014) postulate that structurally similar hillslopes
116 act as functional units for the runoff generation and might thereby be a key unit for
117 understanding catchments of organized complexity (Dooge, 1986). Complementarily,
118 Robinson et al. (1995) showed that the behavior of catchments up to the lower mesoscale
119 are strongly dominated by the hillslope behavior, and Kirkby (1976) highlighted that in
120 catchments extending up to 50 km² random river networks had the same explanative
121 power for runoff generation as the real river network. He concluded that as long as river
122 networks are not dominant the characteristic areas of the catchment hold the key to
123 understand its functioning.

124 In this context it is important to note that a representative hillslope cannot be a simple
125 copy of a real hillslope in a catchment or a simple average of several hillslopes and their
126 structural properties. A much more promising avenue is to set up the representative
127 hillslope based on a perceptual model which is in turn a generalized and simplified
128 picture of the catchment structure and functioning. This is because perceptual models
129 provide a useful means to facilitate communication between field researchers and
130 modelers (Seibert and McDonnell, 2002) and additionally often represent catchments as
131 hillslope-like cross sections. The general idea to translate a perceptual model into a model

structure is not new and has already been applied within a conceptual rainfall-runoff model framework even within the same area (Wrede et al., 2015). The scientific asset of using a physically-based model is that the perceptual model provides important information on typical ordinal differences in hydraulic conductivity of different subsurface strata and the nature and qualitative locations of the dominating preferential flow paths. This information can be implemented into hillslope models in a straightforward manner. The transformation of a qualitative model structure into a quantitative, parametrization of the model depends, however, strongly on the chosen hydrological model and the quality and amount of available data.

Objectives and approach

We hypothesize that a single hillslope in a physically-based model is the most parsimonious representation of a small hilly catchment. The objective of this study is to test this hypothesis in a two-step approach:

- First we derive a qualitative model structure of a representative hillslope from our perception of the dominant processes and the related dominant surface and subsurface characteristics in the catchment.
- In the second step we transform this qualitative model structure into a quantitative model structure without the use of an automatic parameter allocation.

The challenge in deriving a qualitative model structure lies in the separation of the important details from the idiosyncratic ones. This process is to a large extent independent of the chosen hydrological model and is strongly related to the available expert knowledge and quality of the data. The transformation of a qualitative to a quantitative model structure on the other hand depends on the chosen model and whether it is for example based on 2-D or 3-D hillslope module or how rapid flow paths are represented. For this reason the objective of our study is not to “sell” our particular model, but to share the way how we distilled the quantitative model setups in our target catchments from available data and to evaluate the ability of this parsimonious physically-based model to accurately simulate multiple state and flux variables. During the model setup we intendedly avoided using an optimization algorithm to fit the model to the data. In contrary, we relied on various available observations, process-based reasoning, and appropriate literature data for conceiving our perceptual models and parameterizing the representative hillslope models as their quantitative analogues. More specifically, we use geophysical images to constrain subsurface strata and bedrock

165 topography and derived representative soil-water retention curves from a large data set of
166 undisturbed soil samples. Furthermore, we use observations from soil pits, dye staining
167 experiments and observed leaf area indices (LAI) for our model parametrization. Finally
168 we benchmark the hillslope models against normalized double mass curves, the
169 hydrograph as well as against distributed soil moisture and sap flow observations.

170 **2. Study area, data basis and selected model**

171 We focus our model efforts on two different catchments, the Colpach and the
172 Wollefsbach, located in the Attert experimental basins in Luxembourg (Figure 1, Pfister
173 et al., 2000). These sites offer comprehensive laboratory and field data collected by the
174 CAOS (Catchments As Organized Systems) research unit (Zehe et al., 2014). Besides
175 standard hydro-meteorological data the model setup is based on a) observed soil hydraulic
176 properties of a large number of undisturbed soils cores, b) 2-D electric resistivity profiles
177 in combination with soil pits and augering to infer on bedrock topography, and c) flow
178 patterns from dye staining experiments and soil ecological mapping of earthworm
179 burrows, to infer the nature and density of vertical preferential flow paths. The
180 representative hillslopes for the two catchments were each set up as a single 2-D hillslope
181 in the CATFLOW model (Zehe et al., 2001). The following subsections will provide
182 detailed information on the perceptual models and on the water balance of both
183 catchments. We will shortly refer to the key data and those parts of the model which are
184 relevant for the quantitative model setup, while the appendix provides additional details
185 on both.

186 **2.1 The Attert experimental basin**

187 The Attert basin is located in the mid-western part of the Grand-Duchy of Luxembourg
188 and has a total area of 288 km². Mean monthly temperatures range from 18°C in July to a
189 minimum of 0°C in January; mean annual precipitation in the catchment varies around
190 850 mm (1971–2000) (Pfister et al., 2000). The catchment covers three geological
191 formations, the Devonian schists of the Ardennes massif in the northwest, Triassic sandy
192 marls in the center and a small area of sandstone (Jurassic) in the southern part of the
193 catchment (Martínez-Carreras et al., 2012). Our study areas are headwaters named
194 Colpach in the schist area (19.4 km²) and Wollefsbach in the marl area (4.5 km²). As both
195 catchments are located in distinctly different geologies and land use settings, they differ
196 considerably with respect to runoff generation and the dominant controls (e.g. Bos et al.

197 1996, Martínez-Carreras et al. 2012, Fenicia et al. 2014, Wrede et al. 2015, Jackisch
198 2015).

199 **2.1.1 Colpach catchment: perceptual model of structure and functioning**

200 The Colpach catchment has a total area of 19.4 km² and elevation ranges from 265 to 512
201 m a.s.l. It is situated in the northern part of the Attert basin in the Devonian schists of the
202 Ardennes massif. Around 65 % of the catchment are forested, mainly the steep hillslopes
203 (Figure 2). In contrast, the plateaus at the hill tops are predominantly used for agriculture
204 and pasture. Several geophysical experiments and drillings showed that bedrock and
205 surface topography are distinctly different. The bedrock is undulating and rough with
206 ridges, depressions and cracks (compare perceptual model Figure 3 A and ERT image in
207 Figure 6 B). Depressions in the bedrock interface are filled with weathered, silty materials
208 which may form local reservoirs with a high water holding capacity. These reservoirs are
209 connected by a saprolite layer of weathered schist which forms a rapid lateral flow path
210 on top of the consolidated bedrock. Rapid flow in this “bedrock interface” is the dominant
211 runoff process (Wrede et al., 2015), and the specific bedrock topography is deemed to
212 cause typical threshold-like runoff behavior similar to the fill-and-spill mechanism
213 proposed by Tromp-Van Meerveld and McDonnell (2006). Further indication that fill-
214 and-spill is a dominant process is given by the fact that the parent rock is reported as
215 impermeable, which makes deep percolation through un-weathered schist layers into a
216 large groundwater body unlikely (Juilleret et al., 2011). The lack of significant
217 observations of base flow underpins this notion. Furthermore, surface runoff has rarely
218 been observed in the catchment, except along forest roads, which suggests a high
219 infiltrability of the prevailing soils (Bos et al., 1996). This is in line with distributed
220 permeameter measurements and soil sampling performed by Jackisch (2015). Moreover,
221 numerous irrigation and dye staining experiments highlight the important role of vertical
222 structures for rapid infiltration and subsequent subsurface runoff formation (Jackisch
223 2015, Figure 2 B). These vertical preferential flow paths, the saprolite layer on top of the
224 impermeable bedrock, the bedrock topography as well as the absence of a major
225 groundwater body are regarded the dominant structures for the representative hillslope
226 model (Figure 3 A and C).

2.1.2 Wollefsbach catchment: perceptual model of structure and functioning

The Wollefsbach catchment is located in the Triassic sandy marls formation of the Attert basin. It has a size of 4.5 km² and low topographic gradients, with elevation ranging from 245 to 306 m a.s.l. The catchment is intensively used for agriculture and pasture (Figure 2 C); only around 7 % are forested. Hillslopes are often tile-drained (compare perceptual model sketch in Figure 3 B). The heterogeneous marly soils range from sandy loams to thick clay lenses and are generally very silty with high water holding capacities. Similar to the Colpach catchment, vertical preferential flow paths play a major role for the runoff generation; their origin, however, is distinctly different between the seasons. Biogenic macropores are dominant in spring and autumn due to the high abundance of earthworms. Because earthworms are dormant during midsummer and winter, their burrows are partly disconnected by ploughing, shrinking and swelling of the soils (Figure 2 D, see also Figure 4). Soil cracks emerge during long dry spells in midsummer due to the considerable amount of smectite clay minerals in these soils, which drastically increase soil infiltrability in summer (Figure 4). The seasonally varying interaction of both types of preferential flow paths with a dense man-made subsurface drainage network is considered the reason for the flashy runoff regime of this catchment, where discharge rapidly drops to baseflow level when precipitation events end. This is the key feature that needs to be captured by the representative hillslope model. However, as the exact position of the subsurface drainage network and the worm burrows as well as the threshold for soil crack emergence are unknown, the specific influence of each structure on runoff generation in a hydrological model is difficult to estimate.

2.1.3 Water balance and seasonality

The water balance of the Colpach and Wollefsbach catchments for several hydrological years is presented in Figure 5 as normalized double mass curves. Normalized double mass curves relate cumulated runoff to cumulated precipitation, both divided by the sum of the annual precipitation (Pfister et al., 2002, Seibert et al. 2016). Annual runoff coefficients in the Colpach catchment vary around 0.51 ± 0.06 among the four hydrological years (Figure 5 A). Annual runoff coefficients are smaller in the Wollefsbach catchment than in the Colpach catchment, and vary across a wider range, from 0.26 to 0.46 (Figure 5 B). In both catchments the winter period is characterized by step-like changes which reflect fast water release during rainfall events partly due to rapid subsurface flow. In contrast, the

summer regime is characterized by a smooth and almost flat line when vegetation is active. Accumulated rainfall input is not transformed into additional runoff but is either stored in the system or released as evapotranspiration (Jackisch 2015). As suggested by Seibert et al. (2016) we used a temperature index model from Menzel et al. (2003) to detect the bud break of the vegetation and to separate the vegetation-controlled summer regime from the winter period in these curves.

2.2 Data basis

2.2.1 Surface topography and land use

Topographic analyses are based on a 5 m LIDAR digital elevation model which was aggregated and smoothed to 10 m resolution. Land use data from the “Occupation Biophysique du Sol” is based on CORINE land use classes analyzed by color infrared areal images published in 1999 by the Luxembourgian surveying administration “Administration du cadaster et de la Topographie” at a scale of 1:15000.

2.2.2 Subsurface structure and bedrock topography

We used hillslope-scale 2-D electrical resistivity tomography (ERT) in combination with augerings and soil pits to estimate bedrock topography in the schist area. Our auger profiles revealed, in line with Juilleret et al. (2011) and Wrede et al. (2015), that the vertical soil setup comprises a weathered silty soil layer with a downwards increasing fraction of rock fragments, which is underlain by a transition zone of weathered bedrock fragments and by non-weathered and impermeable bedrock. Based on a robust inversion scheme as implemented in Res2Dinv (Loke, 2003) and additional expert knowledge, the subsurface was subdivided into two main layers of unconsolidated material and solid bedrock. The bedrock interface was picked by the 1500 Ωm isoline, as explained in detail in the appendix. For our study we used seven ERT profiles from the Colpach area (example see Figure 6 B).

2.2.3 Soil hydraulic properties

We determined soil texture, saturated hydraulic conductivity and the soil water retention curve for 62 soil samples in the schist area and 25 in the marl area. Particularly for the soil hydraulic functions Jackisch (2015) and Jackisch et al. (2016) found large spatial variability, which was neither explained by slope position nor by the soil depth at which the sample was taken (Figure 7). As our objective was to assess the most parsimonious

representative hillslope model, we neglected this variability but used effective soil water characteristics for both catchments instead. These were not obtained by averaging the parameter of the individual curves, but by grouping the observation points of all soil samples for each geological unit, and averaging them in steps of 0.05 pF. We then fitted a van Genuchten-Mualem model using a maximum likelihood method to these averaged values (Table 1 and Figure 7). The appendix provides additional details on measurement devices and on the dye staining experiments.

2.2.4 Meteorological forcing and discharge

Meteorological data are based on observations from two official meteorological stations (Useldange and Roodt) provided by the “Administration des services techniques de l'agriculture Luxembourg”. Air temperature, relative humidity, wind speed and global radiation are provided with a temporal resolution of 1 h while precipitation data are recorded at an interval of 5 min. Precipitation was extensively quality checked against six disdrometers which are stationed within the Attert basin and by comparing several randomly selected rainfall events against rain radar observations, both using visual inspection. Discharge observations are provided by the Luxembourg Institute of Science and Technology (LIST).

2.2.5 Sap flow and soil moisture data

The Attert basin is instrumented with 45 automated sensor clusters. A single sensor cluster measures inter alia rainfall, and soil moisture in three profiles with sensors at various depths. In this study we use 38 soil moisture sensors located in the schist area and 28 sensors located in the marl area, at depths of 10 and 50 cm. Furthermore we use sap flow measurements from 28 trees at 11 of the sensor cluster sites. The measurement technique is based on the heat ratio method (Burgess et al., 2001), sensors are East30Sensors 3-needle sap flow sensors. As a proxy for sap flow we use the maximum sap velocity of the measurements from three xylem depths (5, 18 and 30 mm) as recorded by each sensor. To represent the daytime flux, we use 12-h daily means between 8am and 8pm.

2.3 The physically-based model CATFLOW

Model simulations were performed using the physically-based hydrological model CATFLOW (Maurer, 1997; Zehe et al., 2001). CATFLOW consists of a 2-D hillslope

321 module which can optionally be combined with a river network to represent a catchment
322 (with several hillslopes). The model employs the standard physically-based approaches to
323 simulate soil water dynamics, optionally solute transport, overland and river flow and
324 evapo-transpiration, which were already mentioned in the introduction and are described
325 in more detail in the appendix. In the following we will only provide details implement of
326 rapid flow paths in the model, as this aspect is differs greatly from model to model.

327 **2.3.1 Generation of rapid vertical and lateral flow paths**

328 Vertical and lateral preferential flow paths are represented as a porous medium with high
329 hydraulic conductivity and very low retention. This approach has already been followed
330 by others (Nieber and Warner 1991; Castiglione et al. 2003; Lamy et al. 2009; Nieber and
331 Sidle 2010), and is one of many ways to account for rapid flow paths in physically-based
332 models. However, it is import to note that such a macropore representation is obviously
333 not an image of the real macropore configuration given the typical grid size of a few
334 centimeters, but a conceptualization to explicitly represent parts of the subsurface with
335 prominent flow paths and the adjacent soil matrix in an effective way. The approach
336 includes the assumption that preserving the connectedness of the rapid flow network
337 (Figure 3) is more important than separating rapid flow and matrix flow into different
338 domains.

339 Implementations of this approach with CATFLOW were successfully used to predict
340 hillslope scale preferential flow and tracer transport in the Weiherbach catchment, a tile-
341 drained agricultural site in Germany (Klaus and Zehe, 2011), and at the Heumöser
342 hillslope, a forested site with fine textured marly soils in Austria (Wienhöfer and Zehe,
343 2014). The locations of vertical macropores along the soil surface may either be selected
344 based on a fixed distance or via a Poisson process based on the surface density of
345 macropores. From these starting points the generator stepwise extends the vertical
346 preferential pathways downwards to a selected depth, while allowing for a lateral step
347 with a predefined probability of typically 0.05 to 0.1 to establish tortuosity. Lateral
348 preferential flow paths to represent either pipes at the bedrock interface or the tile drains
349 are generated in the same manner: starting at the interface to the stream and stepwise
350 extending them upslope, again with a small probability for a vertical upward or
351 downwards step to allow for tortuosity (Figure 3 C and D).

3. Parametrization of the representative hillslope models

3.1 Colpach catchment

3.1.1 Surface topography and spatial discretization

We extracted 241 hillslope profiles based on the available DEM in the Colpach catchment using Whitebox GIS (Lindsay J.B., 2014) following the LUMP approach (Landscape Unit Mapping Program, Francke et al., 2008). Based on these profiles (Figure 6 A) we derived a representative hillslope with a length of 350 m, a maximum elevation of 54 m above the stream, and a total area of 42600 m². The hillslope has a mean slope angle of 11.6° and is facing south (186°), similar to the average aspect of the Colpach catchment. The first step in generating the representative hillslope profile was to calculate the average distance to the river of all 241 extracted hillslope profiles as equal to 380 m. In the next step all elevation and width values of the profiles were binned into 1 m “distance classes” from the river ranging up to the average distance of 380 m. For each class the median values of the a) elevation above the stream and b) the hillslope width were derived and used for the representative hillslope profile (Figure 6 A). For numerical simulation the hillslope was discretized into 766 horizontal and 24 vertical elements with an overall hillslope thickness of 3 m. The vertical grid size was set to 0.128 m, with a reduced vertical grid size of the top node of 0.05 m. Grid size in downslope direction varied between 0.1 m within and close to the rapid flow path and 1 m within reaches without macropores (Figure 3 C). The hillslope thickness of 3 m was chosen to reflect the average of the deepest points of the available bedrock topographies extracted from ERT profiles, which was 2.7 m.

Boundary conditions were set to atmospheric boundary at the top and no flow boundary at the right margin. At the left boundary of the hillslope we selected seepage-boundary condition, where the stored water amount above field capacity leaves the system. A gravitational flow boundary condition was established for the lower boundary. We used spin-up runs with initial states of 70 % of saturation for the entire hydrological year of interest and used the resulting soil moisture pattern for model initialization. This initialization approach was also used for the Wollefsbach catchment.

3.1.2 Land use and vegetation parametrization

According to the land use maps, the hillslopes are mostly forested. As the hilltop plateaus account only for a very small part of the representative hillslope, the land use type for the entire hillslope is set to forest (Figure 2 A). Start and end of the vegetation period was

defined using the temperature-degree model of Menzel et al. (2003), which allowed successful identification of the tipping point between the winter and vegetation season in the double mass curves of the Colpach and of the Wollefsbach (compare Figure 5). We further used observed leaf area indices (LAI) to parameterize the evapotranspiration routine. However, since only fourteen single measurements at different positions are available for the entire schist area and vegetation period, we use the median of all LAI observations from August as a constant value of 6.3 for the vegetation period. To account for the annual pattern of the vegetation phenology we interpolate the LAI for the first and last 30 days of the vegetation period linearly between zero and 6.3, respectively. The other evapotranspiration parameters are displayed in Table 2 and were taken from Breuer et al. (2003) or Schierholz et al. (2000).

3.1.3 Bedrock-topography, permeability and soil hydraulic functions

We used the shape of the bedrock contour line of the ERT image (Figure 6) to constrain the relative topography of the bedrock interface in the hillslope model as follows. We scaled the 100 m of bedrock topography to the hillslope length of 380 m. We then used the average depth to bedrock from all seven available ERT measurements (2.7 m) to scale the maximum depth to bedrock in our model. To this end we divided the average depth of 2.7 m by the deepest point of the bedrock in Figure 6 B (3.3 m) and used the resulting factor of 0.88 to reduce the bedrock depth of Figure 6 B relatively at all positions. As a result, the soil depths to the bedrock interface vary between 1 m to 2.7 m with local depressions that form water holding pools. Since no major groundwater body is suspected and no quantitative data on the rather impermeable schist bedrock in the Colpach is available, we use a relative impermeable bedrock parametrization suggested by Wienhöfer and Zehe (2014, Table 1). It is important to note that due to this bedrock parametrization water flow through the hillslope lower boundary tends to zero.

The silty soil above the bedrock was modeled with the representative hydraulic parameters obtained from field samples listed in Table 1. Since there was no systematic variation of hydraulic parameters of the individual soil samples with depth, soil hydraulic parameters were set constant over depth, except for porosity, which was reduced to a value of 0.35 (m^3m^{-3}) at 50 cm depth to account for the increasing skeleton fraction of around 40% in deeper soil layers.

3.1.4 Rapid subsurface flow paths

Macropore depths were drawn from a normal distribution with a mean of 1 m and a standard deviation of 0.3 m. These values are in agreement with the mean soil depth and correspond well with the results of dye staining experiments performed by Jackisch (2015) and Jackisch et al. (2016). Additionally, macropores were slightly tortuous with a probability for a lateral step of 5 %. Since no observations for the macropore density were available, we use a fixed macropore distance of 2 m. The macropore distance was chosen rather arbitrarily to reflect their relative density in the perceptual model and to establish a partly connected network of vertical and lateral rapid flow paths. The vertical flow paths were parametrized using an artificial porous medium with high hydraulic conductivity and low retention properties proposed by Wienhöfer and Zehe (2014, Table 1). Also the weathered periglacial saprolite layer which is represented by a 0.2 m thick layer above the bedrock was parameterized as a porous medium following Wienhöfer and Zehe, (2014). The estimated saturated hydraulic conductivity of $1 \cdot 10^{-3} \text{ m s}^{-1}$ corresponds well with the velocities described by Angermann et al. (2016). This ensures that the Reynolds number is smaller than 10, implying that flow can be considered laminar and the application of Darcy's law is still appropriate (Bear, 1972).

3.2 Wollefsbach catchment

3.2.1 Surface topography and spatial discretization

Since only eight relatively similar hillslope profiles were derived from the DEM in the Wollefsbach we randomly chose one of those with a length of 653 m, a maximal elevation above the river of 53 m and an area of 373600 m². The hillslope has a mean slope angle of 8.1° and is facing south (172°). The hillslope was discretized into 553 horizontal and 21 vertical elements with an overall hillslope thickness of 2 m (Figure 3 D). The vertical grid size was set to 0.1 m, with a reduced top and bottom node spacing of 0.05 m. Grid size in lateral direction varied between 0.2 m within and close to the rapid flow paths and 2 m within reaches without macropores (Figure 3 B and D).

3.2.2 Land use and vegetation parametrization

Land use was set to grassland within the steeper and lower part of the hillslope, and set to corn for larger distances to the creek (>325 m). Due to the absence of local vegetation data we used tabulated data characterizing grassland and corn from Breuer et al. (2003).

447 Start and end point of the vegetation period for the grassland and the start point for the
448 corn cultivation were again identified by the temperature index model of Menzel et al.
449 (2003). The vegetation period for the corn cultivation ends in the beginning of October
450 since this is the typical period for harvesting. The intra-annual vegetation dynamics were
451 taken from Schierholz et al. (2000).

452 **3.2.3 Bedrock-topography, -permeability and soil hydraulic functions**

453 Contrary to the Colpach, geophysical measurements and augerings revealed bedrock and
454 surface to be more or less parallel. Soil depth was set to constant 1 m and the soil was
455 parameterized using the representative soil retention curves shown in Figure 7. The
456 bedrock was again parameterized according to values Wienhöfer & Zehe (2014) proposed
457 for the impermeable bedrock at the Heumöser hillslope in Austria (Table 1), which is also
458 in a marl geology.

459 **3.2.4 Rapid subsurface flow paths**

460 Based on the perceptual model (Figure 3 B and D) and the reported vertical and lateral
461 drainage structures in the catchment we generated a network of fast flow paths. The
462 depths of the vertical flow paths were drawn from a normal distribution with a mean of
463 0.8 m and a standard deviation of 0.1 m. The tile drain was generated at the standard
464 depth of 0.8 m extending 400 m upslope from the hillslope creek interface. Due to the
465 apparent changes in soil structure either by earthworm burrows or emergent soil cracks
466 (Figure 4), we used different macropore setups for the winter and the vegetation season.
467 For the winter setup we implemented vertical drainage structures every four meters. In the
468 summer setup we added fast flow paths every two meters to account for additional cracks
469 and earthworm burrows. The positions of the conceptual macropores were selected again
470 arbitrarily to create an image of the perceptual model and to assure that the soil surface
471 and the tile drain were well connected. Vertical flow paths and the tile drain were
472 parametrized similar to the Colpach with the same artificial porous medium (Table 1).
473 Boundary conditions of the hillslope, initialization and the spin up phase were the same as
474 described for the Colpach model.

475 **3.3 Model scenarios**

476 Both hillslopes models were set up within a few test simulations to reproduce the
477 normalized double mass curves in both catchments of the hydrological year 2014. We

478 choose the normalized double mass curves as a fingerprint of the annual pattern of runoff
479 generation since it is particular suitable for detecting differences in inter-annual and
480 seasonal runoff dynamics of a catchment (Jackisch, 2015). Model performance was
481 judged by visual inspection as well as by using the Kling-Gupta efficiency (KGE, Gupta
482 et al. 2009).

483 In a second step we compared the simulated overland flow and subsurface storm flow
484 across the left hillslope boundary to observed discharge. Water leaving the hillslope
485 through the lower boundary was neglected from the analysis because in both setups the
486 total amount was smaller than 1 % of the overall hillslope outflow. We compared the
487 specific discharge of the hillslopes to the observed specific discharge of the two
488 catchments in mm h^{-1} by dividing measured and simulated discharge by the area of the
489 catchments and the hillslopes. Our goal was to test if our hillslope models represented the
490 typical subsurface filter properties which are relevant for the runoff generation in both
491 selected hydrological landscapes (schist and marl area in the Attert basin). We measured
492 the model performance with respect to discharge again based on the KGE. Since it is
493 advisable to calculate and display various measures of model performance (Schaeffli and
494 Gupta, 2007), we calculated the Nash-Sutcliffe efficiency (NSE; a measure of model
495 performance with emphasis on high flows) and the logarithmic NSE (log NSE; a
496 performance measure suited for low flows). As both catchments are characterized through
497 a strong seasonality we further separated the simulation period in a winter and vegetation
498 period and calculated the KGE, NSE as well as the logNSE separately for each of the
499 seasons. In addition, we followed Klemesš (1986) and performed a proxy-basin test to
500 check if the runoff simulation is transposable within the same hydrological landscape and
501 conducted a split sampling to examine if the models also work in the hydrological year of
502 2013. Finally, we judged the model goodness visually for selected rainfall-runoff events.

503 In a third step we evaluated the model setups against available soil moisture observations.
504 A natural starting point for a modeling study would be to classify the available soil
505 moisture observation for instance by their landscape position. However, similar to the
506 case of the soil water retention properties, the small scale variability of the soil properties
507 seems to be too dominant, as grouping according to hillslope position was not conclusive
508 (Jackisch, 2015; appendix A4). We therefore extracted simulated soil moisture at 20
509 virtual observation points at different downslope positions at the respective depth of the
510 soil moisture observations (10 and 50 cm), and compared the median of the simulated
511 virtual observations against the 12-hours-rolling median of the observed soil moisture

512 using the KGE and the Spearman rank correlation. Finally, we analyzed simulated
513 transpiration of the Colpach model by plotting it against the 12-hours-rolling median of
514 the daily sap flow velocities observed in the Schist area of the Attert basin. As sap flow is
515 a velocity and transpiration is a normalized flow they are not directly comparable. This is
516 why we normalized both observed sap flow and simulated transpiration by dividing their
517 values by their range and only discuss the correlation among the normalized values. The
518 visual inspection shows additionally to which extent maximum and minimum values of
519 both normalized time series coincide. This cannot be inferred from the correlation
520 coefficient.

521 **4. Results**

522 **4.1 Normalized double mass curves and discharge**

523 The hillslope models reproduce the typical shape of the normalized double mass curves –
524 the steep, almost linear increase in the winter period and the transition to the much flatter
525 summer regime – in both catchments very well (Fig. 8 A, B).

526 The KGEs of 0.92 and 0.9 obtained for the Colpach and the Wollefsbach, respectively,
527 corroborate that within the error ranges both double mass curves are explained well by the
528 models. As a major groundwater body is unlikely in both landscapes, a large inter-annual
529 change in storage is not suspected and we hence state that the hillslope models closely
530 portray the seasonal patterns of the water balance of the catchments. This is further
531 confirmed by the close accordance of simulated and observed annual runoff coefficients.
532 We obtain 0.52 compared to the observed value of 0.55 in the Colpach and 0.39
533 compared to an observed value of 0.42 in the Wollefsbach.

534 In addition to the seasonal water balances, both models also match observed discharge
535 time series in an acceptable manner (KGE 0.88 and 0.71; Table 3). A closer look at the
536 simulated and observed runoff time series (Figure 9 and 10) reveals that the model
537 performance differs in both catchments between the winter and the summer seasons.
538 Generally we observe a better model accordance during the wet winter season, when
539 around 80% of the overall annual runoff is generated in both catchments. In contrast,
540 there are clear deficiencies during dry summer conditions. This is also highlighted by the
541 different performance measures which are in both catchments higher during the winter
542 period than during the vegetation period (Table 3).

543 The Colpach model misses especially the steep and flashy runoff events in June, July and
544 August, and underestimates discharge in summer. It also misses the characteristic double
545 peaks of the catchment as highlighted by runoff events 2 and 3 (Figure 9). Although the
546 model simulates a second peak, it is either too fast (event 2) or the simulated runoff of the
547 second peak is too small (event 3). This finding suggests that our perceptual model of the
548 Colpach catchment needs to be revised, as further elaborated in the discussion. Another
549 shortcoming is the missing snow routine of CATFLOW which can be inferred from event
550 1 (Figure 9 top left panel). While snow is normally not a major control of runoff
551 generation in the rather maritime climate of the Colpach catchment, the runoff event 1
552 happened during temperatures below zero and was most likely influenced by snowfall and
553 subsequent snow melt, which might explain the delay in observed rainfall-runoff
554 response.

555 In the Wollefsbach model the ability to match the hydrograph also differed strongly
556 between the different seasons (Table 3; Figure 10). The flashy runoff response in summer
557 is not always well captured by the model, as for example for a convective rainfall event
558 with rainfall intensities of up to $18 \text{ mm (10 mins)}^{-1}$ in August (Figure 10, event 2).

559 On the contrary, runoff generation during winter is generally simulated acceptably (KGE
560 $= 0.74$). Yet, the model strongly underestimates several runoff events in winter too
561 (Figure 10, event 1). As temperatures during these events were close to zero, this might
562 again be a result of snow accumulation, which cannot be simulated with CATFLOW due
563 to the missing snow routine. It is of key importance to stress that we only achieve
564 acceptable simulations of runoff production in the Wollefsbach when using two different
565 macropore setups for the winter and the summer periods to account for the emergence of
566 cracks (Figure 4) by using a denser 2m-spacing of macropores. When using a single
567 macropore distance of either 2 m (summer setup) or 4 m (winter setup) in the entire
568 simulation period the model shows clear deficits with a KGE of 0.61 and 0.53,
569 respectively. Furthermore, we are able to improve the performance of the Wollefsbach
570 model if we use velocities faster than $1 \cdot 10^{-3} \text{ m/s}$ for the drainage structures. However,
571 this violates the laminar flow assumption and the application of Darcy's law becomes
572 inappropriate.

573 **4.2 Model sensitivities, split sampling and spatial proxy test**

574 Sensitivity tests for the Colpach reveal that the model performance of matching the
575 double mass curves is strongly influenced by the presence of connected rapid flow paths.

576 A complete removal of either the vertical macropores or the bedrock interface from the
577 model domain decreases the model performance considerably (KGE 0.71 or 0.72,
578 respectively). In contrast, reducing the density of vertical macropores from 2 m to 3 or 4
579 m only leads to a slight decrease in model performance (KGE 0.85 and 0.82,
580 respectively). In an additional sensitivity test we changed the bedrock topography from
581 the one inferred from the ERT data to a surface parallel one, which reduces model
582 performance with respect to discharge (KGE < 0.6).

583 The temporal split-sampling reveals that the representative hillslope model of the Colpach
584 also performs well in matching the hydrograph of the previous hydrological year 2012-13
585 (KGE = 0.82). Furthermore, the parameter setup was tested within uncalibrated
586 simulations for the Weierbach catchment (0.45 km²), a headwater of the Colpach in the
587 same geological setting. This again leads to acceptable results (KGE = 0.81, NSE = 0.68).
588 The same applies to the representative hillslope model of the Wollefsbach which also
589 performs well in matching the hydrograph of the previous year (KGE = 0.7).
590 Furthermore, the parameter setup was tested within an uncalibrated simulation for the
591 Schwebich catchment (30 km²), a headwater of the Attert basin in the same geological
592 setting as the Wollefsbach, and again with acceptable results (KGE = 0.81, NSE = 0.7).

593 **4.3 Simulated and observed soil moisture dynamics**

594 We compare the ensemble of soil moisture time series from the virtual observation points
595 to the ensemble of available observations (Figure 11). In the Colpach, soil moisture
596 dynamics are matched well (Spearman rank correlation $r_s = 0.83$). This is further
597 confirmed when comparing this value to the median Spearman rank correlation
598 coefficient of all sensor pairs ($r_s = 0.66$). However, simulated soil moisture at 10 cm
599 depth was systematically higher than the average of the observations. The predictive
600 power in matching the observed average soil moisture dynamics was small (KGE = 0.43;
601 Figure 11 A). Contrary to the positive bias, the total range of the simulated ensemble
602 appears with 0.1 m³ m⁻³ much smaller than the huge spread in the observed time series
603 (0.25 m³ m⁻³). In line with the model performance in simulating discharge, the model has
604 deficiencies in capturing the strong declines in soil moisture in June and July. Simulated
605 soil moisture at 50 cm depth exhibits a strong positive bias and again underestimates the
606 spread in the observed time series. The predictive power is slightly better (KGE = 0.51),
607 while simulated and observed average dynamics are in good accordance ($r_s = 0.89$).

608 Contrary to what we found for the Colpach, the ensemble of simulated soil moisture at 10
 609 cm for the Wollefsbach falls into the state space spanned by the observations; it only
 610 slightly underestimates the rolling median of the observed soil moisture (Figure 11 C. The
 611 predictive power is higher ($KGE = 0.67$) than in the Colpach, while the match of the
 612 temporal dynamics is slightly lower ($r_s = 0.81$). Again the model fails to reproduce the
 613 strong decline in soil moisture between May and July. It is, however, interesting to note
 614 that the model is nearly unbiased during August and September. This is especially
 615 interesting since the Wollefsbach model does not perform too well in simulating
 616 discharge during this time period. Simulated soil moisture at 50 cm depth shows similar
 617 deficiencies as found for the Colpach, while the predictive power was slightly smaller
 618 ($KGE = 0.44$), and also the dynamics is matched slightly worse ($r_s = 0.79$).
 619 When recalling the soil water retention curves (Figure 7), one can infer that a soil water
 620 content of $0.2 \text{ m}^3 \text{ m}^{-3}$ corresponds to pF around 3.8 in the Colpach and to pF around 4.1 in
 621 the Wollefsbach. That in mind it is interesting to note that some observed soil moisture
 622 values are below this threshold throughout the entire year. This is particularly the case for
 623 soil moisture observation at 50 cm depth in the Colpach where almost 50 % of the sensors
 624 measure water contents close to the permanent wilting point throughout the wet winter
 625 period. This also holds true for 8 sensors at 10 cm depth.

626 **4.4 Normalized simulated transpiration versus normalized sap flow velocities**

627 As sap flow provides a proxy for transpiration, we compared normalized, averaged sap
 628 flow velocities of beech and oak trees to the normalized simulated transpiration of the
 629 reference hillslope model of the Colpach. The three-day-rolling-mean of sap flow data
 630 stays close to zero until the end of April and starts to rise after the bud break of the
 631 observed trees. The Colpach model is able to match the bud break of the vegetation well.
 632 Furthermore, simulations and observations are in good accordance during midsummer. In
 633 the period between August and October the simulations underestimate the observations,
 634 while in April and May the simulations are too high (Figure 12). Nevertheless, the model
 635 has some predictive power ($KGE = 0.65$), and is able to mimic the dynamics well ($r_s =$
 636 0.75).

637 **5 Discussion**

638 The presented model results partly corroborate our hypothesis that single representative
639 hillslopes might serve as the most parsimonious representations of two distinctly different
640 lower meso-scale catchments in a physically-based model. The setups of the
641 representative hillslopes were derived as close images of the available perceptual models
642 and by drawing from a variety of field observations, literature data and expert knowledge.
643 The hillslope models were afterwards tested against stream flow data, including a split
644 sampling and a proxy basin test, and against soil moisture and partly against sap flow
645 observations.

646 From the fact that stream flow simulations were acceptable in both catchments when
647 being judged solely on model efficiency criteria, one could conclude that the hillslopes
648 portray the dominant structures and processes which control the runoff generation in both
649 catchments well. A look beyond streamflow-based performance measures revealed,
650 however, clear deficiencies in stream flow simulations during the summer season and
651 during individual rainfall-runoff events as well as a mismatch in simulated soil water
652 dynamics. In the next sections we will hence discuss the strengths and the weaknesses of
653 the representative hillslope model approach. More specifically, in section 5.1 we will
654 focus on the role of soil heterogeneity, preferential flow paths and the added value of
655 geophysical images. In section 5.2 we will discuss the consistency of both models with
656 respect to their ability to reproduce soil moisture and transpiration dynamics. Finally in
657 section 5.3, we discuss if the general idea to picture and model a catchment by a single 2-
658 D representative hillslope is indeed appropriate to simulate the functioning of a lower-
659 mesoscale catchment.

660 **5.1.1 The role of soil heterogeneity for discharge simulations**

661 By using an effective soil water retention curve, instead of accounting for the strong
662 variability of soil hydraulic properties among different soil cores (section 2.2.3) we
663 neglect the stochastic heterogeneity of the soil properties controlling storage and matrix
664 flow. This simplification is a likely reason why the model underestimates the spatial
665 variability in soil moisture time series (compare section 5.2.1). However, our approach
666 does not perform too badly in simulating the normalized double mass curves as well as
667 the runoff generation, at least to some extent, in both catchments. Especially during the
668 winter, when around 80 % of the runoff is generated, runoff is reproduced acceptably

669 well. As our models do not represent the full heterogeneity of the soil water
670 characteristics but are still able to reproduce the runoff dynamics in winter, we reason in
671 line with Ebel and Loague, (2006) that heterogeneity of soil water retention properties is
672 not too important for reproducing the stream flow generation in catchments. In this
673 context it is helpful to recall the fact that hydrological models with three to four
674 parameters are often sufficient to reproduce the stream flow of a catchment. This
675 corroborates that the dimensionality of stream flow is much smaller than one could expect
676 given the huge heterogeneity of the retention properties. This finding has further
677 implications for hydrological modelling approaches as it once more opens the question on
678 the amount of information that is stored in discharge data and how much can be learned
679 when we do hydrology backwards (Jakeman and Hornberger, 1993). Our conclusion
680 should, however, not be misinterpreted that we claim the spatial variability of retention
681 properties to be generally unimportant. The variability of the soil properties of course
682 plays a key role as soon as the focus shifts from catchment-scale runoff generation to
683 solute transport processes, infiltration patterns or to water availability for
684 evapotranspiration.

685 **5.1.2 The role of drainage structures and macropores for discharge simulations**

686 By representing preferential flow paths as connected networks containing an artificial
687 porous medium in the Richards domain, we assume that preserving the connectedness of
688 the network is more important than the separation of rapid flow and matrix flow into
689 different domains. The selected approach was successful in reproducing runoff generation
690 and the water balance for the winter period in the Wollefsbach and Colpach catchments.
691 Simulations with a disconnected network, where either the saprolite layer at the bedrock
692 interface or the vertical macropores were removed, reduced the model performance in the
693 Colpach model from $KGE = 0.88$ to $KGE = 0.6$ and $KGE = 0.71$, respectively. We hence
694 argue that capturing the topology and connectedness of rapid flow paths is crucial for the
695 simulation of stream flow release with representative hillslopes. We furthermore showed
696 that a reduction in the spatial density of macropores from a 2 m to 4 m spacing did not
697 strongly alter the quality of the discharge simulations. This insensitivity can partly be
698 explained by the fact that several configurations of the rapid flow network may lead to a
699 similar model performance. From this insensitivity and the equifinality of the network
700 architecture (Klaus and Zehe, 2010; Wienhöfer and Zehe, 2014) we conclude that it is not
701 the exact position or the exact extent of the macropores which is important for the runoff

702 response but the bare existence of a connected rapid flow path (Jakeman and Hornberger,
703 1993).
704 However, our results also reveal limitations of the representation of rapid flow paths in
705 CATFLOW. For instance model setups with higher saturated hydraulic conductivities
706 ($>10^{-3}$) of the macropore medium clearly improved the model performance in the
707 Wollefsbach but violated the fundamental assumption of Darcy's law of pure laminar
708 flow. This was likely one reason why capturing rapid flow was much more difficult with
709 the selected approach for the Wollefsbach. Another reason was that the emergence of
710 cracks, implying that the relative importance of rapid flow paths for runoff generation is
711 not constant over the year, as highlighted by the findings of dye staining experiments
712 (Figure 4). Given this non-stationary configuration of the macropore network it was
713 indispensable to use a summer and winter configuration to achieve acceptable
714 simulations. This indicates that besides the widely discussed limitations of the different
715 approaches to simulate macropore flow, another challenge is how to deal with emergent
716 behavior and related non-stationary in hydrological model parameters. This is in line with
717 the work of Mendoza et al. (2015), who showed that the agility of hydrological models is
718 often unnecessarily constrained by using static parametrizations. We are aware that the
719 use of a separate model structure in the summer period is clearly only a quick fix, but it
720 highlights the need for more dynamic approaches to account for varying morphological
721 states of the soil structure during long-term simulations.

722 **5.1.3 The role of bedrock topography and water flow through the bedrock**

723 The Colpach model was able to simulate the double peak runoff events which are deemed
724 as typical for this hydrological landscape. However, the model did not perform
725 satisfactorily with regard to peak volume and timing. A major issue that hampers the
726 simulation of these runoff events is that the underlying hydrological processes are still
727 under debate. While Martínez-Carreras et al. (2015) attributes the first peak to water from
728 the riparian zone and the second to subsurface storm flow, other researchers (Angermann
729 et al., 2016; Graeff et al., 2009) suggested that the first peak is caused by subsurface
730 storm flow and the second one by release of groundwater. The representative hillslope
731 model in its present form only allows simulation of overland flow and subsurface storm
732 flow and not the release of groundwater because of the low permeability of the bedrock
733 medium of 10^{-9} m s^{-1} . The deficiency of this model to reproduce double peak runoff
734 events shows that neglecting water flow through the bedrock is possibly not appropriate

(Angermann et al. 2016) and that both the perceptual model and the setup of the representative hillslope for the Colpach need to be refined. We hence suggest that the representative hillslope approach provides an option for a hypothesis-driven refinement of perceptual models, within an iterative learning cycle, until the representative hillslope reproduces the key characteristics one regards as important.

The importance of bedrock topography for the interplay of water flow and storage close to the bedrock was further highlighted by the available 2-D electric resistivity profiles. A model with surface-parallel bedrock topographies performed considerably worse in matching stream flow in terms of the selected performance measures and particularly did not produce the double peak events. This underlines the value of subsurface imaging for process understanding, and is a hint that the Colpach is indeed a fill-and-spill system (Tromp-Van Meerveld and McDonnell, 2006). It also shows that 2-D electric resistivity profiles can be used to constrain bedrock topography in physically-based models (Graeff et al., 2009), which can be of key importance for simulating subsurface storm flow (Hopp and McDonnell, 2009; Lehmann et al., 2006). Although we used constrained bedrock topography only in a straightforward, relative manner in this study, our results corroborated the added value of ERT profiles for hydrological modelling in this kind of hydrological landscapes. Nevertheless, we know that a much more comprehensive study is needed to further detail this finding.

5.2 Integration and use of multi-response and state variables

5.2.1 Storage behavior and soil moisture observations

Both hillslope models reveal much clearer deficiencies with respect to soil moisture observations. While average simulated and observed soil moisture dynamics are partly in good accordance, both models are biased except for the Wollefsbach model at 10 cm depth. In the Wollefsbach catchment this might be explained by the fact that we use an uniform soil porosity for the entire soil profile, although porosity is most likely lower at larger depths for instance due to a higher skeleton fraction. This is no explanation for the Colpach catchment as porosity was reduced in deeper layers with respect to the skeleton fraction. In this context it is interesting to note that quite a few of the soil moisture observations are suspiciously low with average values around 0.2. The resulting pF values of around 3.8 and 4.1 in the Colpach and Wollefsbach, respectively, indicate dry soils even in the wet winter period. This fact has two implications: The first is that the chosen

767 model is almost not capable to simulate such small values, because root water uptake
768 stops at the permanent wilting point and is small at these pF values. The second is that
769 these sensors may have systematic measurement errors, possibly due to entrapped air
770 between the probe and the soil. This entrapped air decreases the dielectric permittivity
771 close to the sensor (Graeff et al., 2010), which implies that measured values will be
772 systematically too low. From this we may conclude that average soil moisture dynamics
773 in both catchments might be higher and the spatial variability of soil moisture time series
774 in turn lower as it appears from the measurements.

775 Additional to the mismatch of the soil moisture simulations, the model fails in
776 reproducing the strong decline in observed soil moisture between May and July 2014. A
777 likely reason for this is that plant roots in the model extract water uniformly within the
778 root zone, while this process is in fact much more variable (Hildebrandt et al., 2015).

779 **5.2.2 Simulated transpiration and sap velocities**

780 It is no surprise that evapotranspiration in our two research catchments is - with a share of
781 around 50 % of the annual water balance - equally important as stream flow. It is also no
782 surprise that evapotranspiration is dominated by transpiration as both catchments are
783 almost entirely covered by vegetation. However, measuring transpiration remains a
784 difficult task, and a lack of reliable transpiration data often hinders the evaluation of
785 hydrological models with respect to this important flux. While it is possible to calculate
786 annual or monthly evapotranspiration sums based on the water balance, more precise
787 information about the temporal dynamics of transpiration is difficult to obtain. Therefore
788 we decided to evaluate our transpiration routine with available sap flow velocity data,
789 because although the absolute values are somewhat error-prone, the dynamics are quite
790 reliable. We tried to account for the uncertainties of the measurements by deriving a
791 three-day-rolling median of 28 observations instead of using single sap flow velocity
792 measurements. As we are comparing sap flow velocity to the simulated transpiration as a
793 normalized flow, we only compare the dynamics of both variables. It is remarkable that
794 despite the uncertainties in the sap flow velocity measurements and our ad-hoc
795 parametrization of the vegetation properties, the comparison of sap flow velocity and
796 simulated transpiration provides additional information, which cannot be extracted from
797 the double mass curve or discharge data. For example, based on the comparison with sap
798 flow velocities we were able to evaluate if the bud break of the dormant trees was
799 specified correctly by the temperature index model of Menzel et al. (2003). Additionally,

we could identify that the spring and autumn dynamics of transpiration, in April as well as in August and September, are matched poorly by the model while the pattern corresponds well in May, June and July. We attribute this discrepancy to the lack of measured LAI values in spring and autumn and to our possibly overly simple vegetation parametrization including several parameters like root depth or plant albedo which are held constant throughout the entire vegetation period. We are aware that this comparison of modeled transpiration with sap flow velocity is only a first, rather simple test; however it encourages the use of sap flow measurements for hydrological modeling. It shows furthermore that the concept of a representative hillslope offers various opportunities for integrating diverse field observations and testing the model's hydrological consistency, for example evaluating it against soil water retention data and sap flow velocities.

5.3 The concept of representative hillslope models

The attempt to model catchment behavior using a two-dimensional representative hillslope implies a symmetry assumption in the sense that the water balance is dominated by the interplay of hillslope parallel and vertical fluxes and the related driving gradients (Zehe et al., 2014). This assumption is corroborated by the acceptable but yet seasonally dependent performance of both hillslope models with respect to matching the water balance and the hydrographs. We particularly learn that the timing of runoff events in these two catchments is dominantly controlled by the structural properties of the hillslopes. This is remarkable for the Colpach catchment which has a size of 19.4 km², but in line with Robinson et al., (1995) who showed that catchments of up to 20 km² can still be hillslope dominated.

An example of the limitations of our single hillslope approach is the deficiency of both models in capturing flashy rainfall-runoff events in the vegetation period. Besides the existence of emergent structures, these events might likely be caused by localized convective storms, probably with a strong contribution of the riparian zones (Martínez-Carreras et al., 2015) and forest roads in the Colpach catchment, and by localized overland flow in the Wollefsbach catchment (Martínez-Carreras et al., 2012). Such fingerprints of a non-uniform rainfall forcing are difficult to be captured by a simulation with a spatially aggregated model; and might require an increase in model complexity. Nevertheless, we suggest that a representative hillslope model provides the right start-up for parameterization of a functional unit when setting up a fully distributed catchment model consisting of several hillslopes and an interconnecting river network. Simulations

833 with distributed rainfall and using the same functional unit parameterization for all
834 hillslopes would tell how the variability in response and storage behavior can be
835 explained compared to the single hillslope. If different functional units are necessary to
836 reproduce the variability of distributed fluxes and storage dynamics, these can for
837 example be generated by stochastic perturbation. We further conclude that the idea of
838 hillslope-scale functional units, which act similarly with respect to runoff generation and
839 might hence serve as building blocks for catchment models, has been corroborated. This
840 is particularly underpinned by the fact that the parameterization of both models was –
841 without tuning – successfully transferred to headwaters in the same geological setting and
842 worked also well for other hydrological years.

843 **6. Conclusions**

844 The exercise to picture and model the functioning of an entire catchment by using a single
845 representative hillslope proved to be successful and instructive. The picturing approach
846 allowed us to consider both quantitative and qualitative information in the physically-
847 based modeling process. This concept made an automated parameter calibration
848 unnecessary and lead to overall acceptable stream flow simulations in two lower-
849 mesoscale catchments. A closer look, however, revealed limitations arising from the
850 drawn perceptual models, the chosen hydrological model or the applicability of the
851 concept itself.

852 Distilling a catchment into a representative hillslope model obviously cannot reflect the
853 entire range of the spatially distributed catchment characteristics. But as the stream flow
854 dynamics of the catchments were simulated reasonably well and the models were even
855 transferable to different catchments it seems that, the use of physically-based models and
856 the large heterogeneities in subsurface characteristics must not prevent meaningful
857 simulations. Additionally, our results highlight the importance of considering non-
858 stationarity of catchment properties in hydrological models on seasonal time scales and
859 emphasize once more the value of multi-response model evaluation. A representative
860 hillslope model for a catchment is, hence, perhaps less accurate than a fully distributed
861 model, but in turn also requires considerably less data and reduced efforts for setup and
862 computation. Therefore, this approach provides a convenient means to test different
863 perceptual models and it can serve as a starting point for increasing model complexity

864 through combination of different hillslopes and a river network to model a catchment in a
865 more distributed manner.
866

867 *Acknowledgements*

868 This research contributes to the “Catchments As Organized Systems (CAOS)” research group (FOR 1598)
869 funded by the German Science Foundation (DFG). Laurent Pfister and Jean-Francois Iffly from the
870 Luxembourg Institute of Science and Technology (LIST) are acknowledged for organizing the permissions
871 for the experiments and providing discharge data for Wollefsbach and Colpach. We also thank the whole
872 CAOS team of phase I & II. Particular we thank Malte Neuper (KIT) for support and discussions on the
873 rainfall data and Markus Weiler, Theresa Blume and Britta Kattenstroth for providing and collecting the
874 soil moisture data. Finally we would like to thank the two anonymous reviewers as they significantly helped
875 to improve and restructure this manuscript.

876

877 **References**

- 878 Angermann, L., Jackisch, C., Allroggen, N., Sprenger, M., Zehe, E., Tronicke, J., Weiler,
879 M. and Blume, T.: In situ investigation of rapid subsurface flow: Temporal dynamics and
880 catchment-scale implication, *Hydrol. Earth Syst. Sci. Discuss.*, 2016(May), 1–34,
881 doi:10.5194/hess-2016-189, 2016.
- 882 Bachmair, S. and Weiler, M.: *Forest Hydrology and Biogeochemistry*, edited by D. F.
883 Levia, D. Carlyle-Moses, and T. Tanaka, Springer Netherlands, Dordrecht., 2011.
- 884 Bear, J.: *Dynamics of Fluids in Porous Media*, American Elsevier, New York., 1972.
- 885 Bergström, S. and Forsman, A.: Development of a conceptual deterministic rainfall-
886 runoff-model, *Hydrol. Res.*, 4(3), 1973.
- 887 Berne, A., Uijlenhoet, R. and Troch, P. A.: Similarity analysis of subsurface flow
888 response of hillslopes with complex geometry, *Water Resour. Res.*, 41(9), n/a–n/a,
889 doi:10.1029/2004WR003629, 2005.
- 890 Beven, K.: Changing ideas in hydrology—the case of physically-based models, *J.*
891 *Hydrol.*, 105, 157–172, 1989.
- 892 Beven, K.: Searching for the Holy Grail of scientific hydrology, , 609–618, 2006a.
- 893 Beven, K.: *Streamflow Generation Processes: Introduction*, 1st edition., edited by K. J.
894 Beven, University of Lancaster, Lancaster, UK., 2006b.
- 895 Beven, K. and Germann, P.: Macropores and water flow in soils revisited, *Water Resour.*
896 *Res.*, 49(6), 3071–3092, doi:10.1002/wrcr.20156, 2013.
- 897 Bishop, J. M., Callaghan, M. V., Cey, E. E. and Bentley, L. R.: Measurement and
898 simulation of subsurface tracer migration to tile drains in low permeability, macroporous
899 soil, *Water Resour. Res.*, 51(6), 3956–3981, doi:10.1002/2014WR016310, 2015.
- 900 Bos, R. van den, Hoffmann, L., Juilleret, J., Matgen, P. and Pfister, L.: Conceptual
901 modelling of individual HRU 's as a trade-off between bottom-up and top-down
902 modelling , a case study ., in *Conf. Environmental Modelling and Software. Proc. 3rd*
903 *Biennal meeting of the international Environmental Modelling and Software Society.*
904 *Vermont, USA.*, 1996.
- 905 Breuer, L., Eckhardt, K. and Frede, H.-G.: Plant parameter values for models in temperate

- 906 climates, *Ecol. Modell.*, 169(2-3), 237–293, doi:10.1016/S0304-3800(03)00274-6, 2003.
- 907 Bronstert, A. and Plate, E. J.: Modelling of runoff generation and soil moisture dynamics
 908 for hillslopes and micro-catchments, *J. Hydrol.*, 198(1-4), 177–195, doi:10.1016/S0022-
 909 1694(96)03306-9, 1997.
- 910 Brunner, P. and Simmons, C. T.: HydroGeoSphere: A Fully Integrated, Physically Based
 911 Hydrological Model, *Ground Water*, 50(2), 170–176, doi:10.1111/j.1745-
 912 6584.2011.00882.x, 2012.
- 913 Burgess, S. S., Adams, M. a, Turner, N. C., Beverly, C. R., Ong, C. K., Khan, a a and
 914 Bleby, T. M.: An improved heat pulse method to measure low and reverse rates of sap
 915 flow in woody plants., *Tree Physiol.*, 21(9), 589–598, doi:10.1093/treephys/21.9.589,
 916 2001.
- 917 Camporese, M., Paniconi, C., Putti, M. and Orlandini, S.: Surface-subsurface flow
 918 modeling with path-based runoff routing, boundary condition-based coupling, and
 919 assimilation of multisource observation data, *Water Resour. Res.*, 46(2),
 920 doi:10.1029/2008WR007536, 2010.
- 921 Celia, M. A., Bouloutas, E. T. and Zarba, R. L.: A general mass-conservative numerical
 922 solution for the unsaturated flow equation, *Water Resour. Res.*, 26(7), 1483–1496,
 923 doi:10.1029/WR026i007p01483, 1990.
- 924 Coenders-Gerrits, A. M. J., Hopp, L., Savenije, H. H. G. and Pfister, L.: The effect of
 925 spatial throughfall patterns on soil moisture patterns at the hillslope scale, *Hydrol. Earth
 926 Syst. Sci.*, 17(5), 1749–1763, doi:10.5194/hess-17-1749-2013, 2013.
- 927 Dooge, J. C. I.: Looking for hydrologic laws, *Water Resour. Res.*, 22(9), 46S,
 928 doi:10.1029/WR022i09Sp0046S, 1986.
- 929 Dunne, T. and Black, R. D.: Partial Area Contributions to Storm Runoff in a Small New
 930 England Watershed, *Water Resour. Res.*, 6(5), 1296–1311,
 931 doi:10.1029/WR006i005p01296, 1970.
- 932 Ebel, B. a. and Loague, K.: Physics-based hydrologic-response simulation: Seeing
 933 through the fog of equifinality, *Hydrol. Process.*, 20(13), 2887–2900,
 934 doi:10.1002/hyp.6388, 2006.
- 935 Ebel, B. a., Loague, K., Montgomery, D. R. and Dietrich, W. E.: Physics-based
 936 continuous simulation of long-term near-surface hydrologic response for the Coos Bay
 937 experimental catchment, *Water Resour. Res.*, 44(7), 1–23, doi:10.1029/2007WR006442,
 938 2008.

- 939 Fenicia, F., Kavetski, D., Savenije, H. H. G., Clark, M. P., Schoups, G., Pfister, L. and
 940 Freer, J.: Catchment properties, function, and conceptual model representation: is there a
 941 correspondence?, *Hydrol. Process.*, 28(4), 2451–2467, doi:10.1002/hyp.9726, 2013.
- 942 Francke, T., Güntner, a., Mamede, G., Müller, E. N. and Bronstert, a.: Automated
 943 catena-based discretization of landscapes for the derivation of hydrological modelling
 944 units, *Int. J. Geogr. Inf. Sci.*, 22(2), 111–132, doi:10.1080/13658810701300873, 2008.
- 945 Freeze, R. A. and Harlan, R. L.: Blueprint for a physically-based, digitally-simulated
 946 hydrologic response model, *J. Hydrol.*, 9(3), 237–258, doi:10.1016/0022-1694(69)90020-
 947 1, 1969.
- 948 Graeff, T., Zehe, E., Reusser, D., Lück, E., Schröder, B., Wenk, G., John, H. and
 949 Bronstert, A.: Process identification through rejection of model structures in a mid-
 950 mountainous rural catchment: observations of rainfall-runoff response, geophysical
 951 conditions and model inter-comparison, *Hydrol. Process.*, 23(5), 702–718,
 952 doi:10.1002/hyp.7171, 2009.
- 953 Graeff, T., Zehe, E., Schlaeger, S., Morgner, M., Bauer, A., Becker, R., Creutzfeldt, B.
 954 and Bronstert, A.: A quality assessment of Spatial TDR soil moisture measurements in
 955 homogenous and heterogeneous media with laboratory experiments, *Hydrol. Earth Syst.*
 956 *Sci.*, 14(6), 1007–1020, doi:10.5194/hess-14-1007-2010, 2010.
- 957 Grayson, R. B., Moore, I. D. and McMahon, T. A.: Physically based hydrologic
 958 modeling: 2. Is the concept realistic?, *Water Resour. Res.*, 28(10), 2659–2666,
 959 doi:10.1029/92WR01259, 1992.
- 960 Gupta, H. V., Kling, H., Yilmaz, K. K. and Martinez, G. F.: Decomposition of the mean
 961 squared error and NSE performance criteria: Implications for improving hydrological
 962 modelling, *J. Hydrol.*, 377(1-2), 80–91, doi:10.1016/j.jhydrol.2009.08.003, 2009.
- 963 Gupta, H. V., Clark, M. P., Vrugt, J. a., Abramowitz, G. and Ye, M.: Towards a
 964 comprehensive assessment of model structural adequacy, *Water Resour. Res.*, 48(8), 1–
 965 16, doi:10.1029/2011WR011044, 2012.
- 966 Hazenberg, P., Broxton, P., Gochis, D., Niu, G.-Y., Pangle, L. A., Pelletier, J. D., Troch,
 967 P. A. and Zeng, X.: Testing the hybrid-3-D hillslope hydrological model in a controlled
 968 environment, *Water Resour. Res.*, 52(2), 1089–1107, doi:10.1002/2015WR018106, 2016.
- 969 Hildebrandt, A., Kleidon, A. and Bechmann, M.: A thermodynamic formulation of root
 970 water uptake, *Hydrol. Earth Syst. Sci. Discuss.*, 12(12), 13383–13413, doi:10.5194/hessd-
 971 12-13383-2015, 2015.

- 972 Hopp, L. and McDonnell, J. J.: Connectivity at the hillslope scale: Identifying interactions
973 between storm size, bedrock permeability, slope angle and soil depth, *J. Hydrol.*, 376(3-
974 4), 378–391, doi:10.1016/j.jhydrol.2009.07.047, 2009.
- 975 Hopp, L., Harman, C., Desilets, S., Graham, C., McDonnell, J. and Troch, P.: Hillslope
976 hydrology under glass: confronting fundamental questions of soil-water-biota co-
977 evolution at Biosphere 2, *Hydrol. Earth Syst. Sci. Discuss.*, 6(3), 4411–4448,
978 doi:10.5194/hessd-6-4411-2009, 2009.
- 979 Jackisch, C.: Linking structure and functioning of hydrological systems., KIT -
980 Karlsruher Institut of Technology., 2015.
- 981 Jackisch, C., Angermann, L., Allroggen, N., Sprenger, M., Blume, T., Weiler, M.,
982 Tronicke, J. and Zehe, E.: In situ investigation of rapid subsurface flow: Identification of
983 relevant spatial structures beyond heterogeneity, *Hydrol. Earth Syst. Sci. Discuss.*, 2016,
984 1–32, doi:10.5194/hess-2016-190, 2016.
- 985 Jakeman, A. J. and Hornberger, G. M.: How much complexity is warranted in a rainfall-
986 runoff model?, *Water Resour. Res.*, 29(8), 2637–2649, doi:10.1029/93WR00877, 1993.
- 987 Jarvis, P. G.: The Interpretation of the Variations in Leaf Water Potential and Stomatal
988 Conductance Found in Canopies in the Field, *Philos. Trans. R. Soc. B Biol. Sci.*,
989 273(927), 593–610, doi:10.1098/rstb.1976.0035, 1976.
- 990 Juilleret, J., Iffly, J. F., Pfister, L. and Hissler, C.: Remarkable Pleistocene periglacial
991 slope deposits in Luxembourg (Oesling): pedological implication and geosite potential,
992 *Bull. la Société des Nat. Luxemb.*, 112(1), 125–130, 2011.
- 993 Kirkby, M.: Tests of the random network model, and its application to basin hydrology,
994 *Earth Surf. Process.*, 1(August 1975), 197–212, doi:10.1002/esp.3290010302, 1976.
- 995 Klaus, J. and Zehe, E.: Modelling rapid flow response of a tile-drained field site using a
996 2D physically based model: assessment of “equifinal” model setups, *Hydrol. Process.*,
997 24(12), 1595–1609, doi:10.1002/hyp.7687, 2010.
- 998 Klaus, J. and Zehe, E.: A novel explicit approach to model bromide and pesticide
999 transport in connected soil structures, *Hydrol. Earth Syst. Sci.*, 15(7), 2127–2144,
1000 doi:10.5194/hess-15-2127-2011, 2011.
- 1001 Klemeš, V.: Operational testing of hydrological simulation models, *Hydrol. Sci. J.*, 31(1),
1002 13–24, doi:10.1080/02626668609491024, 1986.

- 1003 Lee, H., Zehe, E. and Sivapalan, M.: Predictions of rainfall-runoff response and soil
1004 moisture dynamics in a microscale catchment using the CREW model, *Hydrol. Earth*
1005 *Syst. Sci. Discuss.*, 3(4), 1667–1743, doi:10.5194/hessd-3-1667-2006, 2006.
- 1006 Lehmann, P., Hinz, C., McGrath, G., Tromp-van Meerveld, H.-J. and McDonnell, J. J.:
1007 Rainfall threshold for hillslope outflow: an emergent property of flow pathway
1008 connectivity, *Hydrol. Earth Syst. Sci. Discuss.*, 3(5), 2923–2961, doi:10.5194/hessd-3-
1009 2923-2006, 2006.
- 1010 Lindsay J.B.: The Whitebox Geospatial Analysis Tools project and open-access GIS,
1011 *Proc. GIS Res. UK 22nd Annu. Conf.*, (001), 8, doi:10.13140/RG.2.1.1010.8962, 2014.
- 1012 Loague, K. and VanderKwaak, J. E.: Physics-based hydrologic response simulation:
1013 Platinum bridge, 1958 Edsel, or useful tool, *Hydrol. Process.*, 18(15), 2949–2956,
1014 doi:10.1002/hyp.5737, 2004.
- 1015 Loke, M.: Rapid 2D Resistivity & IP Inversion using the least-squares method, *Geotomo*
1016 *Software, Man.*, 2003.
- 1017 Martínez-Carreras, N., Krein, A., Gallart, F., Iffly, J.-F., Hissler, C., Pfister, L.,
1018 Hoffmann, L. and Owens, P. N.: The Influence of Sediment Sources and Hydrologic
1019 Events on the Nutrient and Metal Content of Fine-Grained Sediments (Attert River Basin,
1020 Luxembourg), *Water, Air, Soil Pollut.*, 223(9), 5685–5705, doi:10.1007/s11270-012-
1021 1307-1, 2012.
- 1022 Martínez-Carreras, N., Wetzel, C. E., Frentress, J., Ector, L., McDonnell, J. J., Hoffmann,
1023 L. and Pfister, L.: Hydrological connectivity inferred from diatom transport through the
1024 riparian-stream system, *Hydrol. Earth Syst. Sci.*, 19(7), 3133–3151, doi:10.5194/hess-19-
1025 3133-2015, 2015.
- 1026 Maurer, T.: Physikalisch begründete zeitkontinuierliche Modellierung des
1027 Wassertransports in kleinen ländlichen Einzugsgebieten., *Karlsruher Institut für*
1028 *Technologie.*, 1997.
- 1029 Mendoza, P. A., Clark, M. P., Barlage, M., Rajagopalan, B., Samaniego, L., Abramowitz,
1030 G. and Gupta, H.: Are we unnecessarily constraining the agility of complex process-based
1031 models?, *Water Resour. Res.*, 51(1), 716–728, doi:10.1002/2014WR015820, 2015.
- 1032 Menzel, A., Jakobi, G., Ahas, R., Scheifinger, H. and Estrella, N.: Variations of the
1033 climatological growing season (1951-2000) in Germany compared with other countries,
1034 *Int. J. Climatol.*, 23(7), 793–812, doi:10.1002/joc.915, 2003.
- 1035 Mueller, E. N., Güntner, A., Francke, T. and Mamede, G.: Modelling sediment export,

- 1036 retention and reservoir sedimentation in drylands with the WASA-SED model, *Geosci.*
1037 *Model Dev.*, 3(1), 275–291, doi:10.5194/gmd-3-275-2010, 2010.
- 1038 Niu, G.-Y., Yang, Z.-L., Mitchell, K. E., Chen, F., Ek, M. B., Barlage, M., Kumar, A.,
1039 Manning, K., Niyogi, D., Rosero, E., Tewari, M. and Xia, Y.: The community Noah land
1040 surface model with multiparameterization options (Noah-MP): 1. Model description and
1041 evaluation with local-scale measurements, *J. Geophys. Res.*, 116(D12), D12109,
1042 doi:10.1029/2010JD015139, 2011.
- 1043 Pérez, A. J., Abrahão, R., Causapé, J., Cirpka, O. A. and Bürger, C. M.: Simulating the
1044 transition of a semi-arid rainfed catchment towards irrigation agriculture, *J. Hydrol.*,
1045 409(3-4), 663–681, doi:10.1016/j.jhydrol.2011.08.061, 2011.
- 1046 Peters, A. and Durner, W.: Simplified evaporation method for determining soil hydraulic
1047 properties, *J. Hydrol.*, 356(1-2), 147–162, doi:10.1016/j.jhydrol.2008.04.016, 2008.
- 1048 Pfister, L., Humbert, J. and Hoffmann, L.: Recent trends in rainfall-runoff characteristics
1049 in the Alzette River basin, Luxembourg, *Clim. Change*, 45(1996), 323–337,
1050 doi:10.1023/A:1005567808533, 2000.
- 1051 Pfister, L., Iffly, J.-F., Hoffmann, L. and Humbert, J.: Use of regionalized stormflow
1052 coefficients with a view to hydroclimatological hazard mapping, *Hydrol. Sci. J.*, 47(3),
1053 479–491, doi:10.1080/02626660209492948, 2002.
- 1054 Refsgaard, J. and Storm, B.: MIKE SHE in Computer models of watershed hydrology,
1055 edited by V. P. Singh, Water Resources Publications., 1995.
- 1056 Refsgaard, J. C., Thorsen, M., Jensen, J. B., Kleeschulte, S. and Hansen, S.: Large scale
1057 modelling of groundwater contamination from nitrate leaching, *J. Hydrol.*, 221(3-4), 117–
1058 140, doi:10.1016/S0022-1694(99)00081-5, 1999.
- 1059 Reggiani, P. and Rientjes, T. H. M.: Flux parameterization in the representative
1060 elementary watershed approach: Application to a natural basin, *Water Resour. Res.*,
1061 41(4), n/a–n/a, doi:10.1029/2004WR003693, 2005.
- 1062 Robinson, J. S., Sivapalan, M. and Snell, J. D.: On the relative roles of hillslope
1063 processes, channel routing, and network geomorphology in the hydrologic response of
1064 natural catchments, *Water Resour. Res.*, 31(12), 3089–3101, doi:10.1029/95WR01948,
1065 1995.
- 1066 Savenije, H. H. G. and Hrachowitz, M.: Opinion paper: How to make our models more
1067 physically-based, *Hydrol. Earth Syst. Sci. Discuss.*, 0(August), 1–23, doi:10.5194/hess-
1068 2016-433, 2016.

- 1069 Schaeffli, B. and Gupta, H. V: Do Nash values have value?, *Hydrol. Process.*, 21(15),
1070 2075–2080, doi:10.1002/hyp.6825, 2007.
- 1071 Schierholz, I., Schäfer, D. and Kolle, O.: The Weiherbach data set: An experimental data
1072 set for pesticide model testing on the field scale, *Agric. Water Manag.*, 44(1-3), 43–61,
1073 doi:10.1016/S0378-3774(99)00083-9, 2000.
- 1074 Schoups, G., Van De Giesen, N. C. and Savenije, H. H. G.: Model complexity control for
1075 hydrologic prediction, in *Water Resources Research.*, 2008.
- 1076 Scudeler, C., Pangle, L., Pasetto, D., Niu, G.-Y., Volkmann, T., Paniconi, C., Putti, M.
1077 and Troch, P.: Multiresponse modeling of an unsaturated zone isotope tracer experiment
1078 at the Landscape Evolution Observatory, *Hydrol. Earth Syst. Sci. Discuss.*, (May), 1–29,
1079 doi:10.5194/hess-2016-228, 2016.
- 1080 Seibert, J. and McDonnell, J. J.: On the dialog between experimentalist and modeler in
1081 catchment hydrology: Use of soft data for multicriteria model calibration, *Water Resour.*
1082 *Res.*, 38(11), 23–1–23–14, doi:10.1029/2001WR000978, 2002.
- 1083 Seibert, S. P., Ehret, U. and Zehe, E.: Disentangling timing and amplitude errors in
1084 streamflow simulations, *Hydrol. Earth Syst. Sci. Discuss.*, (March), 1–37,
1085 doi:10.5194/hess-2016-145, 2016.
- 1086 Simunek, J., Genuchten, M. Van and Sejna, M.: The HYDRUS software package for
1087 simulating the two-and three-dimensional movement of water, heat, and multiple solutes
1088 in variably-saturated media, *Tech. Man.*, 2006.
- 1089 Troch, P., Paniconi, C. and Loon, E. Van: Hillslope-storage Boussinesq model for
1090 subsurface flow and variable source areas along complex hillslopes: 1. Formulation and
1091 characteristic response, *Water Resour. Res.*, 39(11), 1316, 2003.
- 1092 Tromp-Van Meerveld, H. J. and McDonnell, J. J.: Threshold relations in subsurface
1093 stormflow: 2. The fill and spill hypothesis, *Water Resour. Res.*, 42(August 2005), 1–11,
1094 doi:10.1029/2004WR003800, 2006.
- 1095 Wienhöfer, J. and Zehe, E.: Predicting subsurface stormflow response of a forested
1096 hillslope – the role of connected flow paths, *Hydrol. Earth Syst. Sci.*, 18(1), 121–138,
1097 doi:10.5194/hess-18-121-2014, 2014.
- 1098 Wrede, S., Fenicia, F., Martínez-Carreras, N., Juilleret, J., Hissler, C., Krein, A., Savenije,
1099 H. H. G., Uhlenbrook, S., Kavetski, D. and Pfister, L.: Towards more systematic
1100 perceptual model development: a case study using 3 Luxembourgish catchments, *Hydrol.*
1101 *Process.*, 29(12), 2731–2750, doi:10.1002/hyp.10393, 2015.

- 1102 Zehe, E. and Sivapalan, M.: Editorial Towards a new generation of hydrological process
1103 models for the meso-scale: an introduction, 2007.
- 1104 Zehe, E., Maurer, T., Ihringer, J. and Plate, E.: Modeling water flow and mass transport in
1105 a loess catchment, *Phys. Chem. Earth, Part B Hydrol. Ocean. Atmos.*, 26(7-8), 487–507,
1106 doi:10.1016/S1464-1909(01)00041-7, 2001.
- 1107 Zehe, E., Becker, R., Bárdossy, A. and Plate, E.: Uncertainty of simulated catchment
1108 runoff response in the presence of threshold processes: Role of initial soil moisture and
1109 precipitation, *J. Hydrol.*, 315(1-4), 183–202, doi:10.1016/j.jhydrol.2005.03.038, 2005.
- 1110 Zehe, E., Lee, H. and Sivapalan, M.: Dynamical process upscaling for deriving catchment
1111 scale state variables and constitutive relations for meso-scale process models, *Hydrol.*
1112 *Earth Syst. Sci.*, 10(6), 981–996, doi:10.5194/hess-10-981-2006, 2006.
- 1113 Zehe, E., Graeff, T., Morgner, M., Bauer, A. and Bronstert, A.: Plot and field scale soil
1114 moisture dynamics and subsurface wetness control on runoff generation in a headwater in
1115 the Ore Mountains, *Hydrol. Earth Syst. Sci.*, 14(6), 873–889, doi:10.5194/hess-14-873-
1116 2010, 2010.
- 1117 Zehe, E., Ehret, U., Blume, T., Kleidon, a., Scherer, U. and Westhoff, M.: A
1118 thermodynamic approach to link self-organization, preferential flow and rainfall–runoff
1119 behaviour, *Hydrol. Earth Syst. Sci.*, 17(11), 4297–4322, doi:10.5194/hess-17-4297-2013,
1120 2013.
- 1121 Zehe, E., Ehret, U., Pfister, L., Blume, T., Schröder, B., Westhoff, M., Jackisch, C.,
1122 Schymanski, S. J., Weiler, M., Schulz, K., Allroggen, N., Tronicke, J., Dietrich, P.,
1123 Scherer, U., Eccard, J., Wulfmeyer, V. and Kleidon, A.: HESS Opinions: Functional
1124 units: a novel framework to explore the link between spatial organization and
1125 hydrological functioning of intermediate scale catchments, *Hydrol. Earth Syst. Sci.*
1126 *Discuss.*, 11(3), 3249–3313, doi:10.5194/hessd-11-3249-2014, 2014.
- 1127 Zhang, G. P. and Savenije, H. H. G.: Rainfall-runoff modelling in a catchment with a
1128 complex groundwater flow system: application of the Representative Elementary
1129 Watershed (REW) approach, *Hydrol. Earth Syst. Sci. Discuss.*, 2(3), 639–690,
1130 doi:10.5194/hessd-2-639-2005, 2005.

1131

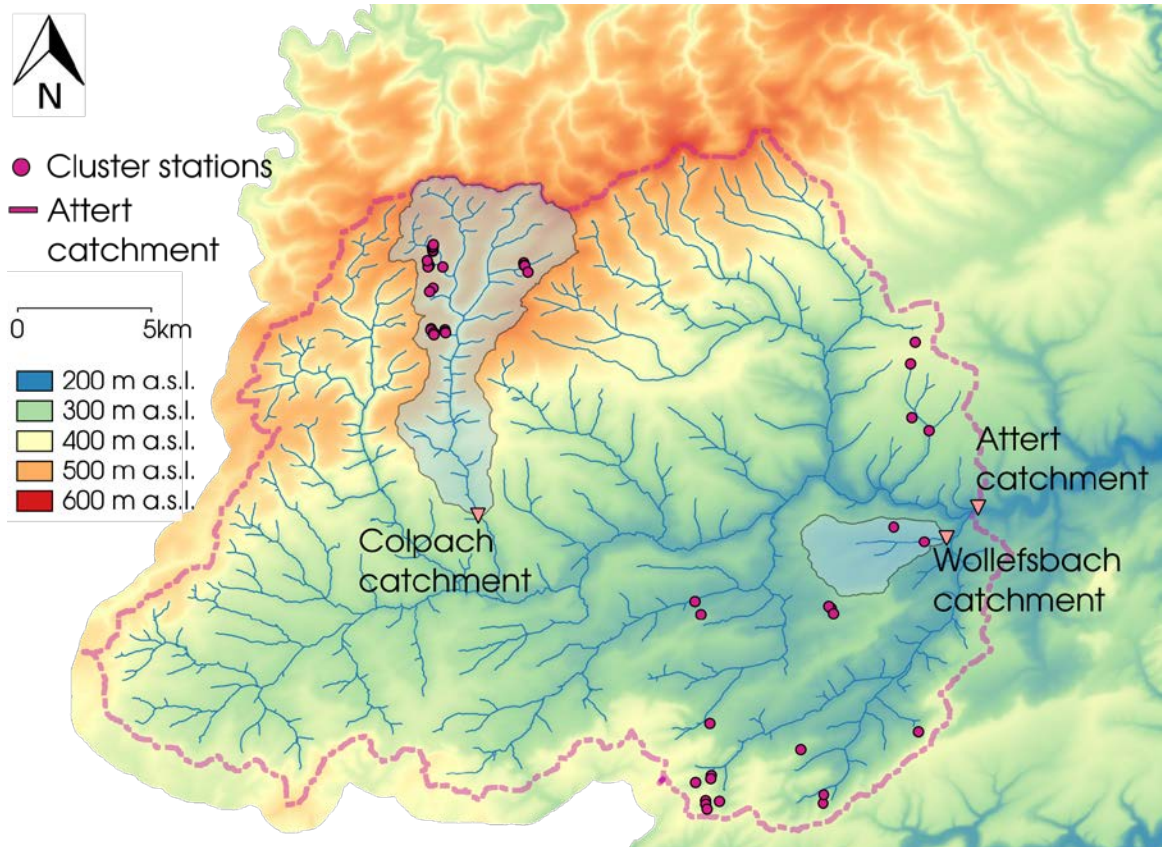
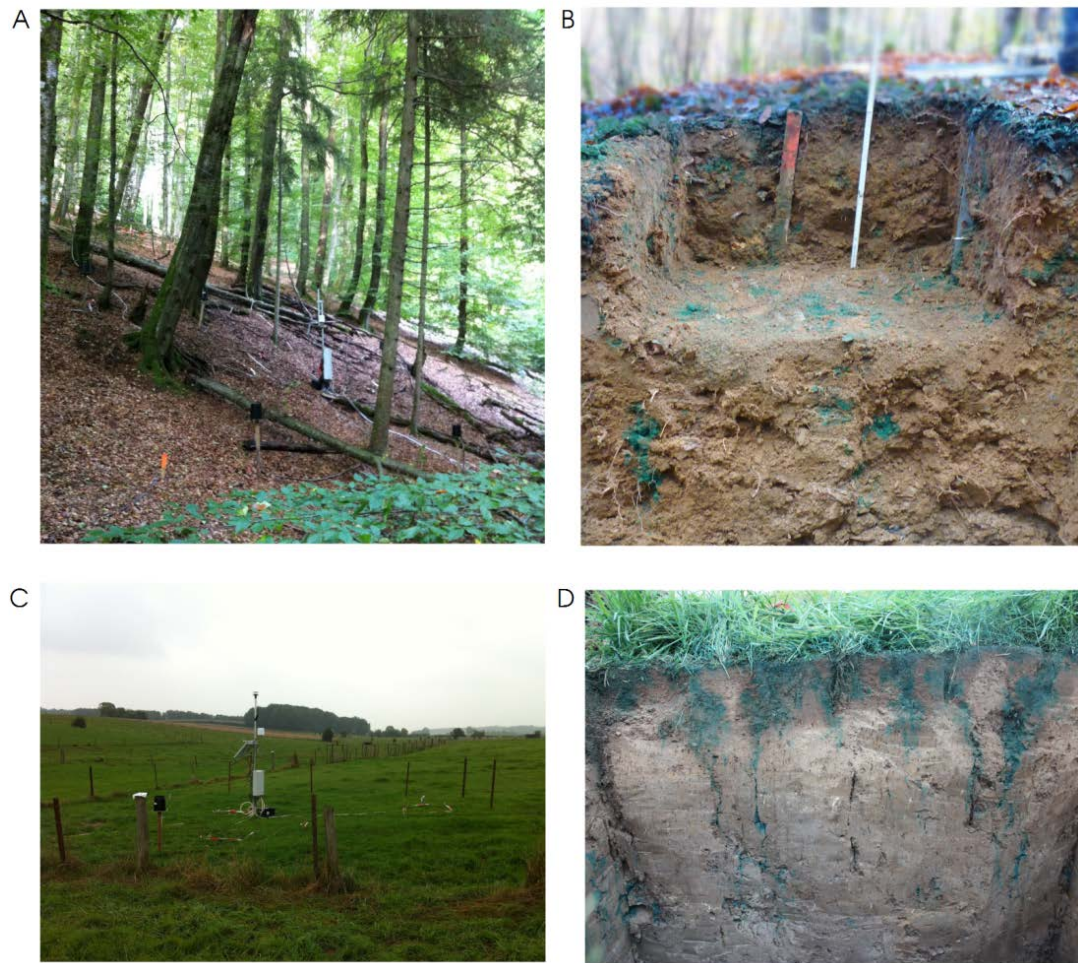


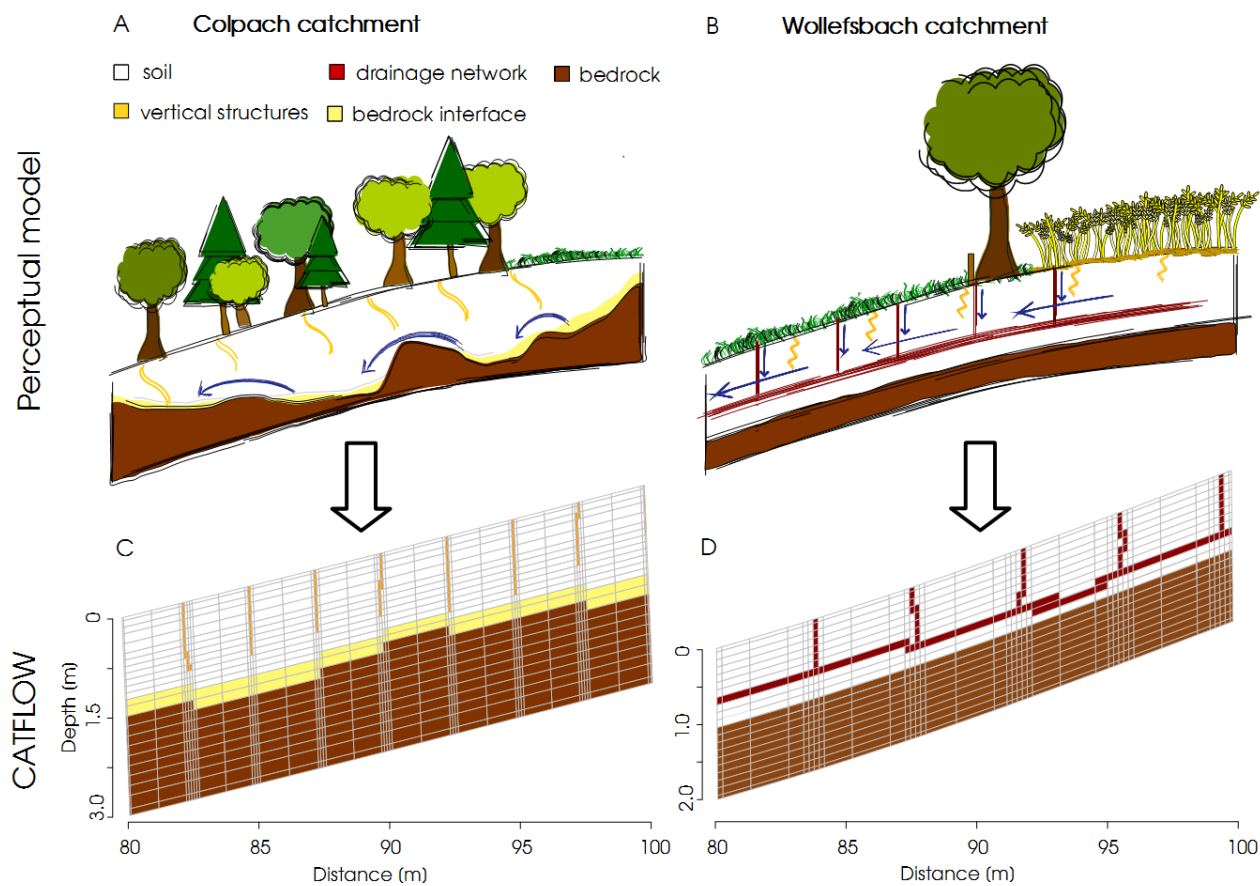
Figure 1 Map of the Atttert basin with the two selected headwater catchments of this study (Colpach and Wollefsbach). In addition, the cluster sites of the CAOS research unit are displayed.



1137

1138 **Figure 2 (A) Typical steep forested hillslope in the Colpach catchment; (B) Soil profile in the Colpach catchment**
 1139 **after a brilliant blue sprinkling experiment was conducted. The punctual appearance of blue color illustrates the**
 1140 **influence of vertical structures on soil water movement in this schist area. (C) Plain pasture site of the**
 1141 **Wollefsbach catchment; (D) Soil profile in the Wollefsbach catchment after a brilliant blue experiment showing**
 1142 **the influence of soil cracks and vertical structures on the soil water movement.**

1143



1144

1145 **Figure 3** Perceptual models of the (A) Colpach and (B) Wollefsbach and their translation into a representative
1146 hillslope model for CATFLOW. It is important to note that only small sections of the model hillslope are
1147 displayed (C Colpach; D Wollefsbach) and not the entire hillslope.

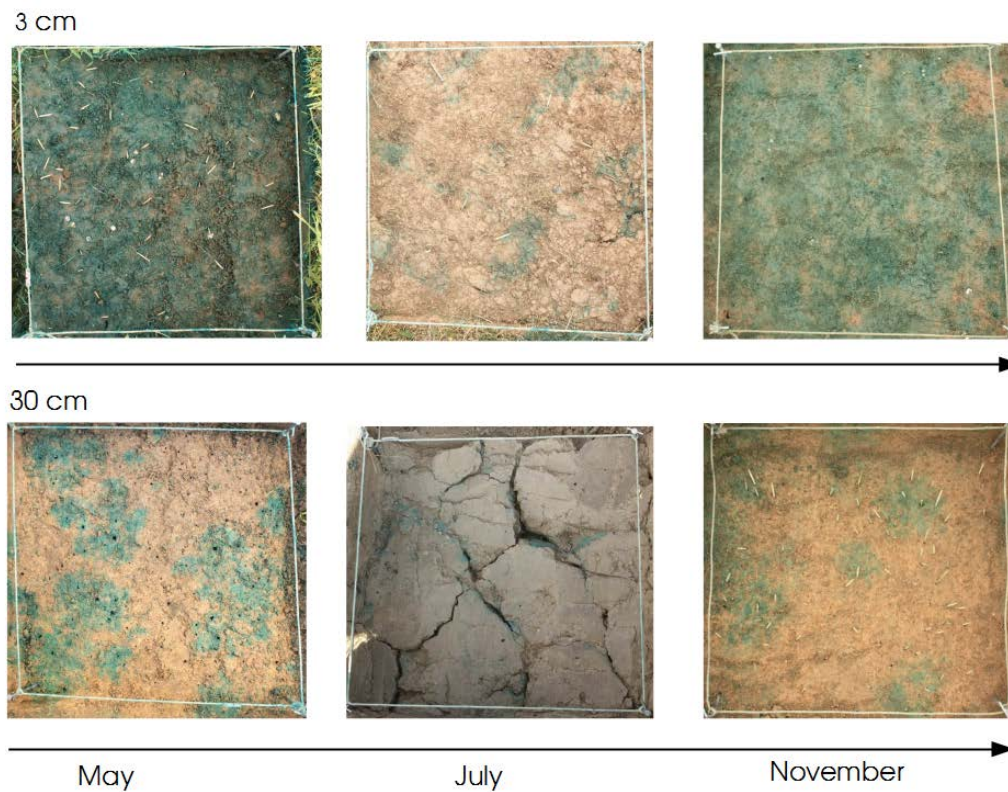
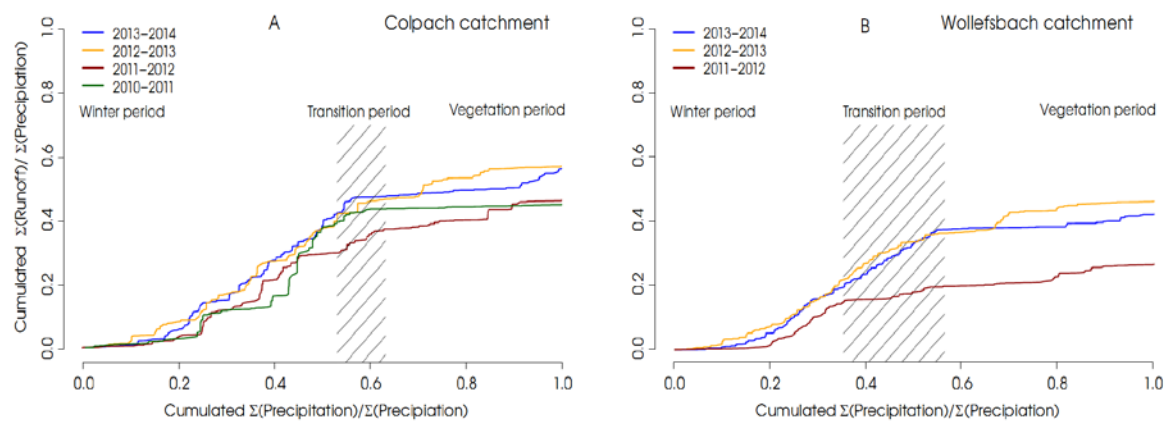


Figure 4 Emergent structures in the Wollefsbach catchment for the sampling dates. In May macropore flow through earth worm burrows dominates infiltration, while in July clearly visible soil cracks occur. In contrast, a more homogenous infiltration pattern is visible in November, especially at 3 cm depth.

1153

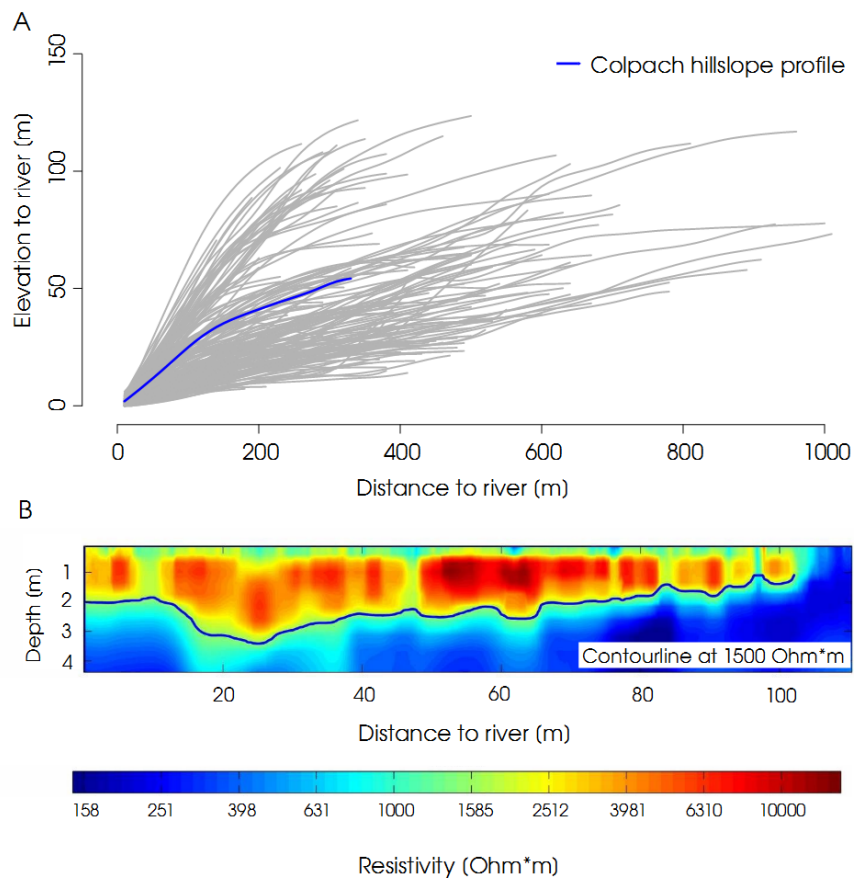


1154

1155 **Figure 5** Normalized double mass curves for each hydrological year from 2010 to 2014 in the Colpach catchment
1156 **(A)** and from 2011 to 2014 in the Wollefsbach catchment **(B)**. The transition period marks the time of the years
1157 **when the catchment shifts from the winter period to the vegetation period. The separation of the seasons is based**
1158 **on a temperature index model from Menzel et al., (2003). Since the season shift varies between the hydrological**
1159 **years the transition period is displayed as an area.**

1160

1161



1162

1163 **Figure 6 (A) Profile of all hillslope extracted from a DEM in the Colpach catchment. Hillslope profile we used in**
 1164 **this study highlighted in blue. (B) Bedrock topography of a hillslope in the Schist area measured using ERT. The**
 1165 **contour line displays the 1500 Ω m isoline which is interpreted as soil bedrock interface.**

1166

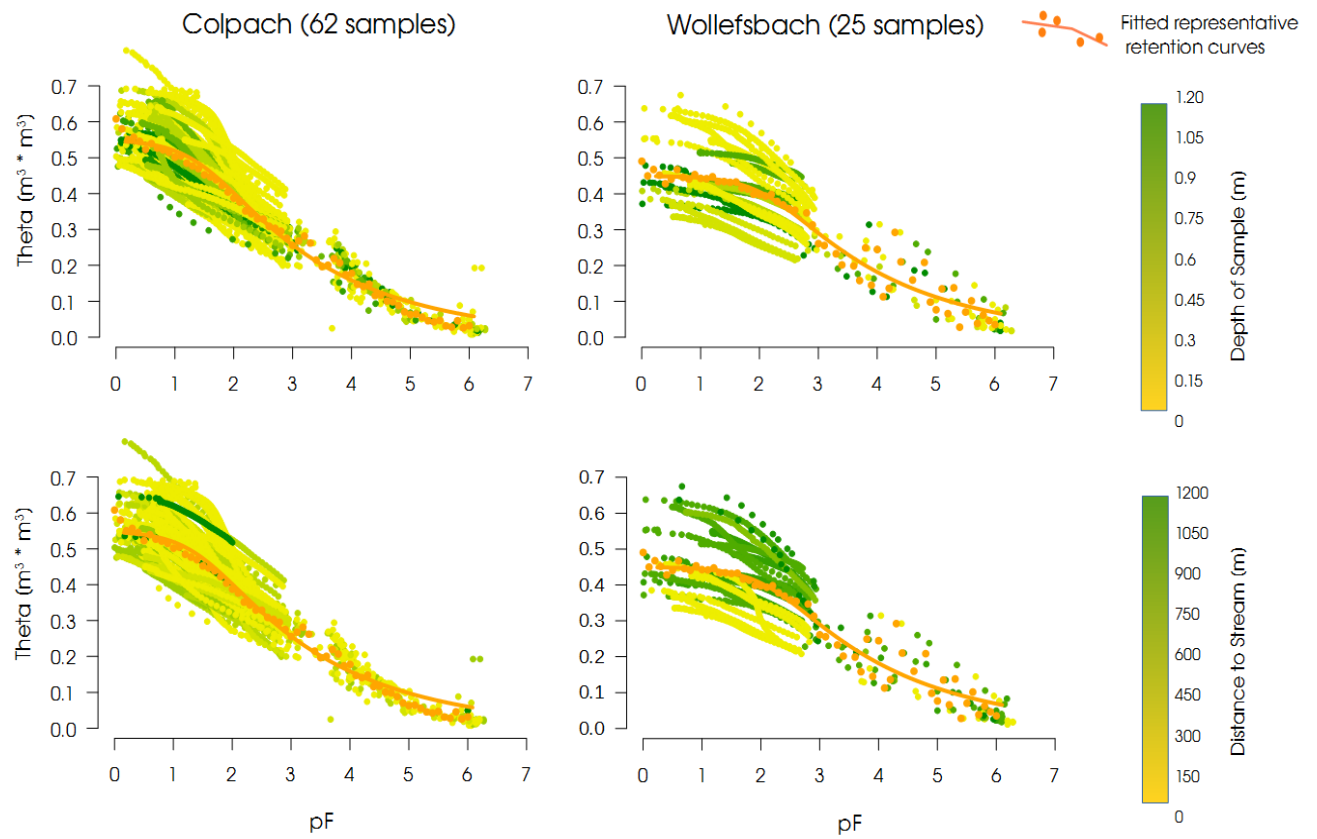
1167

1168

1169

1170

1171

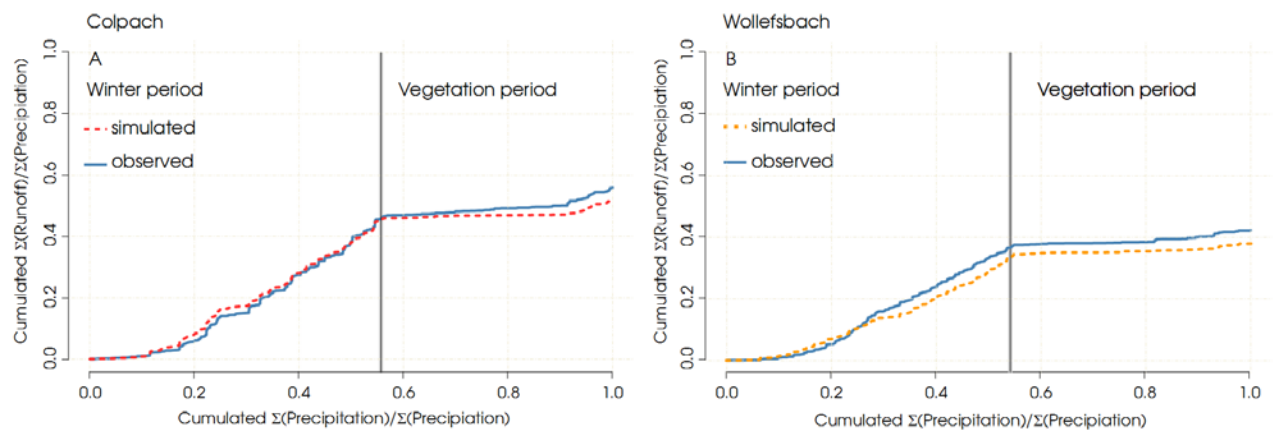


1172

1173 **Figure 7 Fitted soil water retention curves and measured soil water retention relationships for the Colpach (A)**
 1174 **and Wollefsbach (B) catchment.**

1175

1176

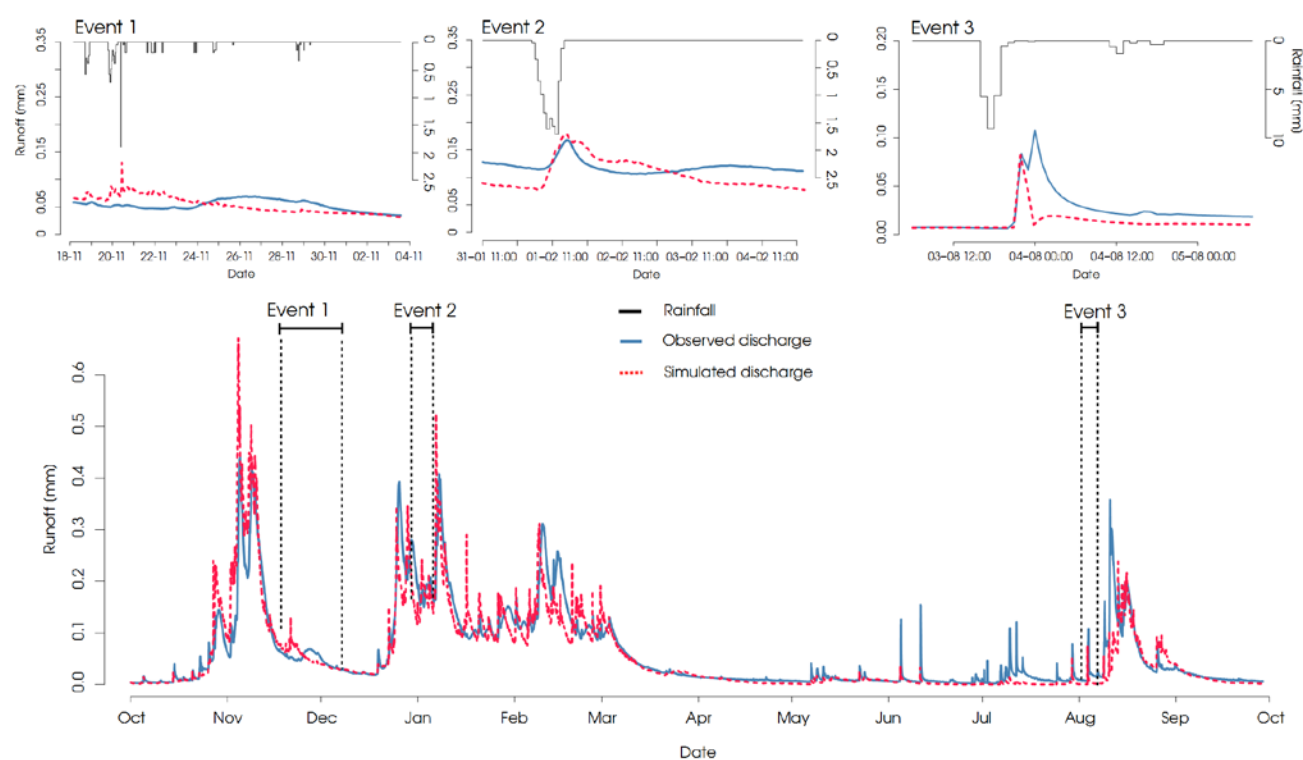


1177

1178 **Figure 8 Simulated and observed normalized double mass curves of (A) the Colpach and (B) the Wollefsbach**
 1179 **catchment. The double mass curves are separated into a winter and a vegetation period after Menzel et al.**
 1180 **(2003).**

1181

1182



1183

1184 **Figure 9** Observed and simulated runoff of the Colpach catchment. Moreover, three rainfall runoff events are
1185 highlighted and displayed separately.

1186

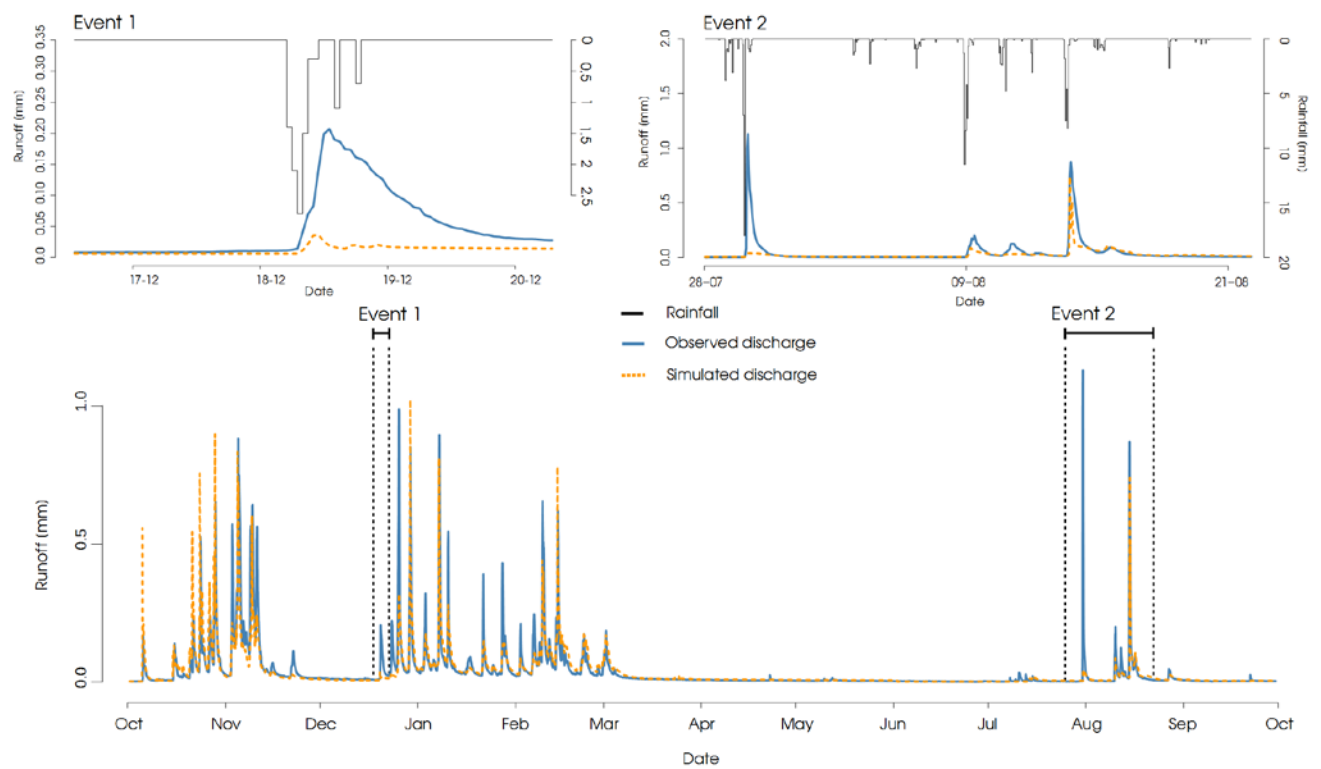
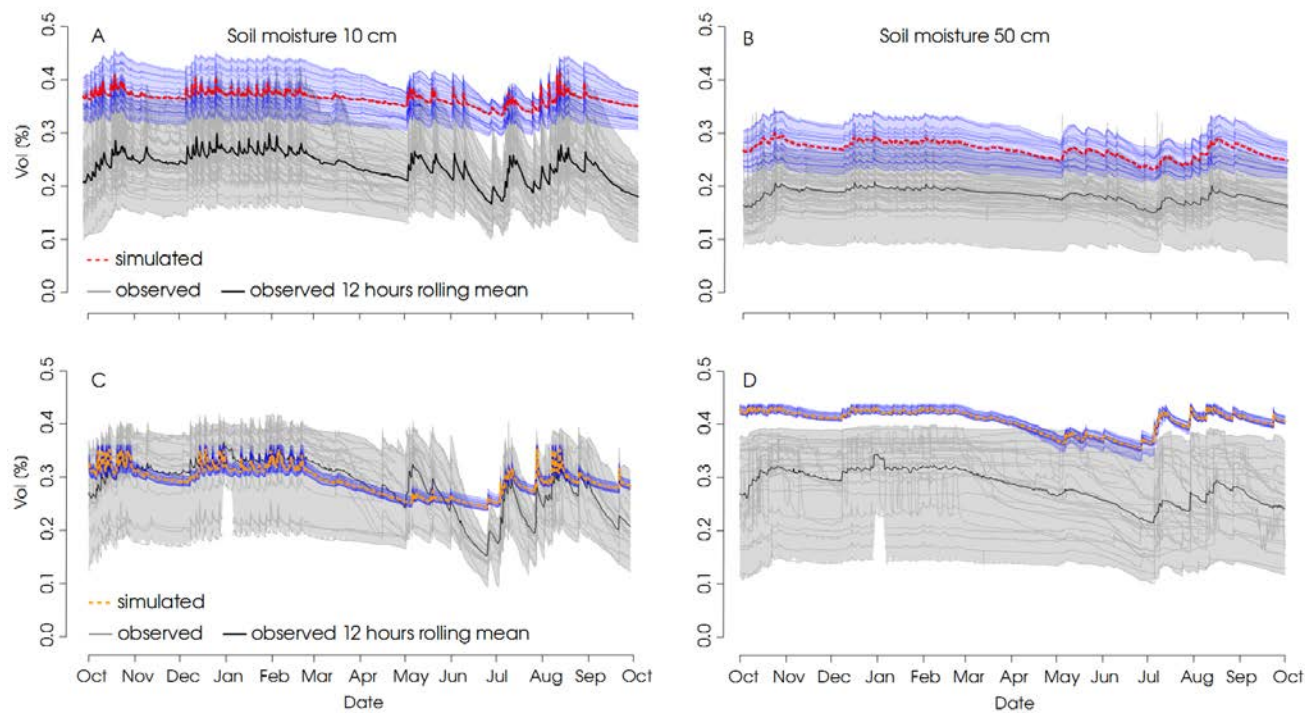


Figure 10 Observed and simulated runoff of the Wollefsbach catchment. Two rainfall runoff events are highlighted and displayed separately.

1191

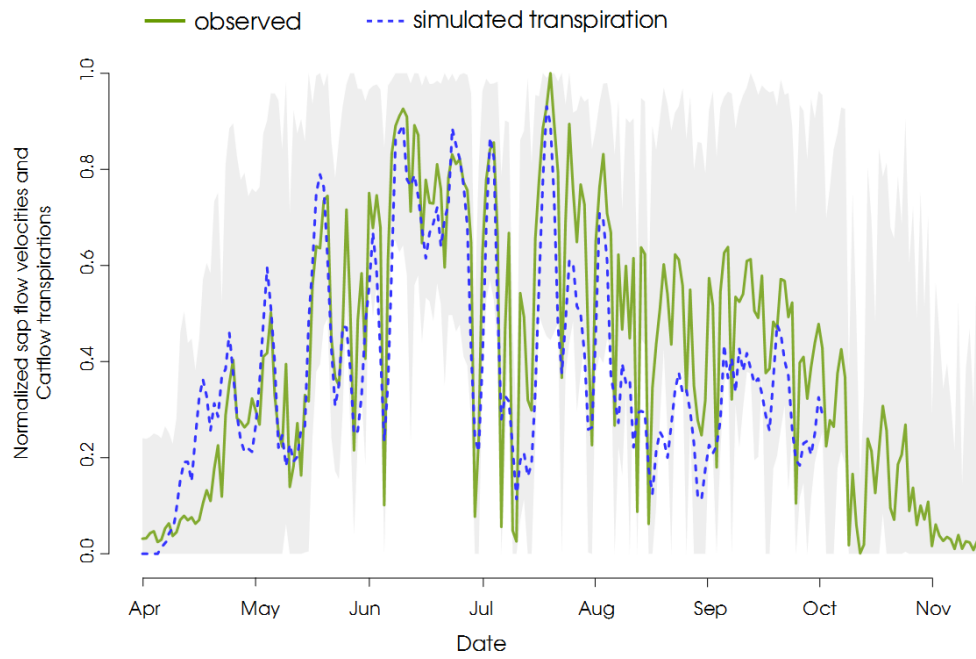


1192

1193 **Figure 11** Observed soil moisture at 10 and 50 cm depths in the schist (A and B) and marl (C and D) area of the
1194 Attert catchment. Additionally the 12 hours rolling median (black) derived from the soil moisture observations
1195 and the simulated soil moisture dynamics at the respective depths (red Colpach; orange Wollefsbach) are
1196 displayed.

1197

1198



1199

1200 **Figure 12** Normalized observed average sap velocities of 28 trees in the Colpach catchment (green) and
1201 normalized simulated transpiration from the Colpach model smoothed with a three-day rolling mean (dashed
1202 blue). Additionally the ensemble of all 28 sap flow measurements is displayed in grey.

1203

1204 **Table 1 Hydraulic and transport parameter values used for different materials in the model setups.**

Type of structure	Saturated hydraulic conductivity K_s (m s ⁻¹)	Total porosity Θ_s (-)	Residual water content Θ_r (-)	Alpha value α (m ⁻¹)	Shape parameter n (-)
<i>Colpach</i>					
Soil layer	5×10 ⁻⁴	0.57	0.05	4.93	1.05
Macropores & soil bedrock interface	1×10 ⁻³	0.25	0.1	7.5	1.5
Bedrock	1×10 ⁻⁹	0.2	0.05	0.5	2
<i>Wollefsbach</i>					
Soil layer	2.92×10 ⁻⁴	0.46	0.05	0.66	1.05
Drainage system	1×10 ⁻³	0.25	0.1	7.5	1.5
Bedrock	1×10 ⁻⁹	0.2	0.05	0.5	2

1205
1206
1207

1208 **Table 2 Vegetation parameter values for the different land use forms in the model setup.**

	Start / End of the Vegetatio n period [doy]	LAI [-]	Root depth [m]	Through fall rate [%]	Plant height [m]	Intercepti on [mm]	Maximum stomata conductance [mm s ⁻¹]	Albedo [-]
Colpach:								
Forest (<i>Fagus sylvatica</i>)	97 / 307	6.3 ⁴	1.8	95	24 ⁴	2	5	0.2
Wollefsbach								
Corn (<i>Zea mays</i>)	97 / 307	4 ²	1.2 ¹	100	2	3	2.5	0.2
Pasture	97 / 274	6 ²	1.3 ³	100	0.4	3.1 ³	2.5	0.2

1209 ¹ value for gley brown soils; ² mean value (Breuer et al., 2003); ³ Trifolium spec., ⁴ observed

1210

1211 **Table 3 Benchmarks for simulated double mass curves and simulated discharge for all model setups used in this**
1212 **study.**

Model setup	<i>Double mass curve:</i>	<i>Discharge:</i>		
	KGE	KGE	NSE	logNSE
<i>Colpach models</i>				
Reference Colpach model:	0.92	0.88	0.79	0.25
Performance winter :	0.95	0.88	0.75	0.93
Performance summer:	0.49	0.52	0.51	0.62
<i>Wollefsbach models</i>				0.87
Reference Wollefsbach model:	0.9	0.71	0.68	0.84
Peformance winter:	0.85	0.74	0.7	0.57
Performance summer:	0.74	0.28	0.33	

1213

1214

1215 **Appendix**

1216 **A1 Subsurface structure and bedrock topography**

1217 Spatial subsurface information of representative hillslopes were obtained from 2-D ERT
1218 sections collected using a GeoTom (GeoLog) device at seven profiles on two hillslopes in
1219 the Colpach catchment. We used a Wenner configuration with electrode spacing of 0.5 m
1220 and 25 depth levels: electrode positions were recorded at a sub-centimeter accuracy using
1221 a total station providing 3D position information. Application of a robust inversion
1222 scheme as implemented in Res2Dinv (Loke, 2003) resulted in the two-layered subsurface
1223 resistivity model shown in Figure 6 B. The upper 1-3 m are characterized by high
1224 resistivity values larger than $1500 \Omega \cdot \text{m}$. This is underlain by a layer of generally lower
1225 resistivity values smaller than $1500 \Omega \cdot \text{m}$. In line with the study of Wrede et al. (2015)
1226 and in correspondence with the maximum depth of the local auger profiles, we interpreted
1227 the transition from high to low resistivity values to reflect the transition zone between
1228 bedrock and unconsolidated soil. In consequence, we regard the $1500 \Omega \text{m}$ isoline as being
1229 representative for the soil-bedrock interface. For our modeling study we have access to
1230 seven ERT profiles within the Colpach area (example see Figure 6 B).

1231 **A2 Soil hydraulic properties, infiltrability and dye staining experiments**

1232 Saturated hydraulic conductivity was measured with undisturbed 250 ml ring samples
1233 with the KSAT apparatus (UMS GmbH). The apparatus records the falling head of the
1234 water supply through a highly sensitive pressure transducer which is used to calculate the
1235 flux. The soil water retention curve of the drying branch was measured with the same
1236 samples in the HYPROP apparatus (UMS GmbH) and subsequently in the WP4C dew
1237 point hygrometer (Decagon Devices Inc.). The HYPROP records total mass and matric
1238 head in two depths in the sample over some days when it was exposed to free evaporation
1239 (Peters and Durner, 2008, Jackisch 2015 for further details). For both geological settings
1240 we estimated a mean soil retention curve by grouping the observation points of all soil
1241 samples (62 and 25 for schist and marl, respectively), and averaging them in steps of 0.05
1242 pF. We then fitted a van Genuchten-Mualem model using a maximum likelihood method
1243 to these averaged values (Table 1 and Figure 7). We used a representative soil water
1244 retention curve because the young soils on periglacial slope deposits prevail in the both
1245 headwaters exhibit large heterogeneity which cannot be grouped in a simple manner. This
1246 is due to a) the general mismatch of the scale of 250 mL undisturbed core samples with

the relevant flow paths and b) the high content of gravel and voids, which affect the retention curve especially above field capacity and concerning its scaling with available pore space (Jackisch 2015, Jackisch et al. 2016). The dye tracer images, Figure 2 B and D, were obtained with high rainfall intensities of 50 mm in 1 h on 1 m² and the sprinkling water was enriched with 4.0 g l⁻¹ Brilliant Blue dye tracer (Jackisch et al. 2016). The aim of these rainfall simulations was to visualize the macropore networks in the topsoil, to gather information on the potential preferential flow paths relevant for infiltration.

A3 Physically-based model CATFLOW

The model CATFLOW has been successfully used and specified in numerous studies (e.g. Zehe et al., 2005; Zehe et al. 2010; Wienhöfer and Zehe, 2014; Zehe et al., 2014). The basic modeling unit is a two-dimensional hillslope. The hillslope profile is discretized by curvilinear orthogonal coordinates in vertical and downslope directions; the third dimension is represented via a variable width of the slope perpendicular to the slope line at each node. Soil water dynamics are simulated based on the Richards equation in the pressure based form and numerically solved using an implicit mass conservative “Picard iteration” (Celia et al., 1990). The model can simulate unsaturated and saturated subsurface flow and hence has no separate groundwater routine. Soil hydraulic functions after van Genuchten-Mualem are commonly used, though several other parameterizations are possible. Overland flow is simulated using the diffusion wave approximation of the Saint-Venant equation and explicit upstreaming. The hillslope module can simulate infiltration excess runoff, saturation excess runoff, re-infiltration of surface runoff, lateral water flow in the subsurface as well as return flow. For catchment modeling several hillslopes can be interconnected by a river network for collecting and routing their runoff contributions, i.e. surface runoff or subsurface flow leaving the hillslope, to the catchment outlet. CATFLOW has no routine to simulate snow or frozen soil.

A3.1 Evaporation controls, root water uptake and vegetation phenology

Soil evaporation, plant transpiration and evaporation from the interception store is simulated based on the Penman–Monteith equation. Soil moisture dependence of the soil albedo is also accounted for as specified in Zehe et al. (2001). Annual cycles of plant phenological parameters, plant albedo and plant roughness are accounted for in the form of tabulated data (Zehe et al., 2001). Optionally, the impact of local topography on wind speed and on radiation may be considered, if respective data are available. The

atmospheric resistance is equal to wind speed in the boundary layer over the squared friction velocity [mm d^{-1}]. The former depends on observed wind speed, plant roughness and thus plant height. The friction velocity depends on observed wind speed as well as atmospheric stability, which is represented through six stability classes depending on prevailing global radiation, air temperature and humidity. The canopy resistance is the product of leaf area index and leaf resistance, which in turn depends on stomata and cuticular resistance. The stomata resistance varies around a minimum value, which depends on the Julian day as well as on air temperature, water availability in the root zone, the water vapor saturation deficit and photosynthetic active radiation (Jarvis, (1976). The resulting root water uptake is accounted for as a sink in the Richards equations term, and is specified as a flux per volume, which is extracted uniformly along the entire root depth.

A4 Soil moisture observations

Figure A1 shows the soil moisture observations of the Colpach catchment group by their position at the hillslope. This figure highlight, similar to Figure 7 for the soil water retention properties, that the small-scale variability of the prevailing soils make a simple grouping by the landscape position difficult.

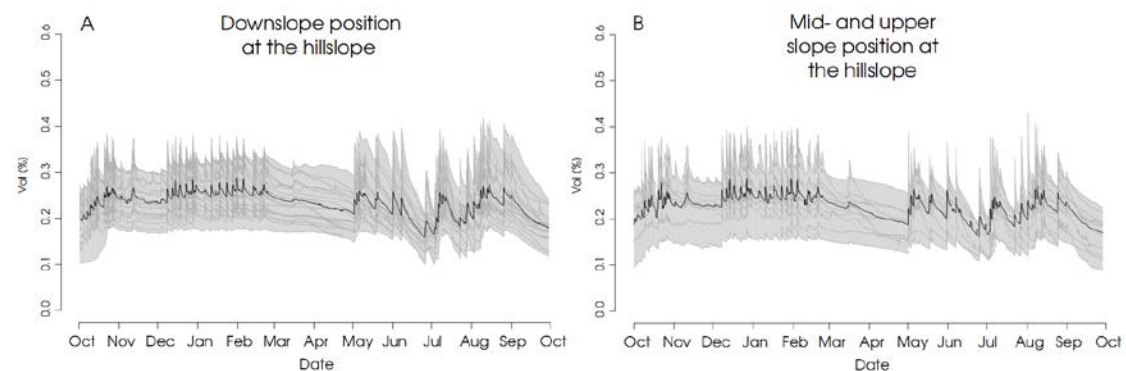


Figure A1 Soil moisture observations grouped by their landscape position. (A) Soil moisture observations at the hillslope foot and hence close to the river. (B) Soil moisture observations at the upper part of the hillslope.